INDIVIDUAL TREE DELINEATION FROM HIGH RESOLUTION SAR IMAGE USING THE SCALE-SPACE BLOB METHOD

SEPIDEH KIA
Enschede, The Netherlands, February 2019

SUPERVISORS:
Dr. V. Tolpekin
Dr. Y. Hussin

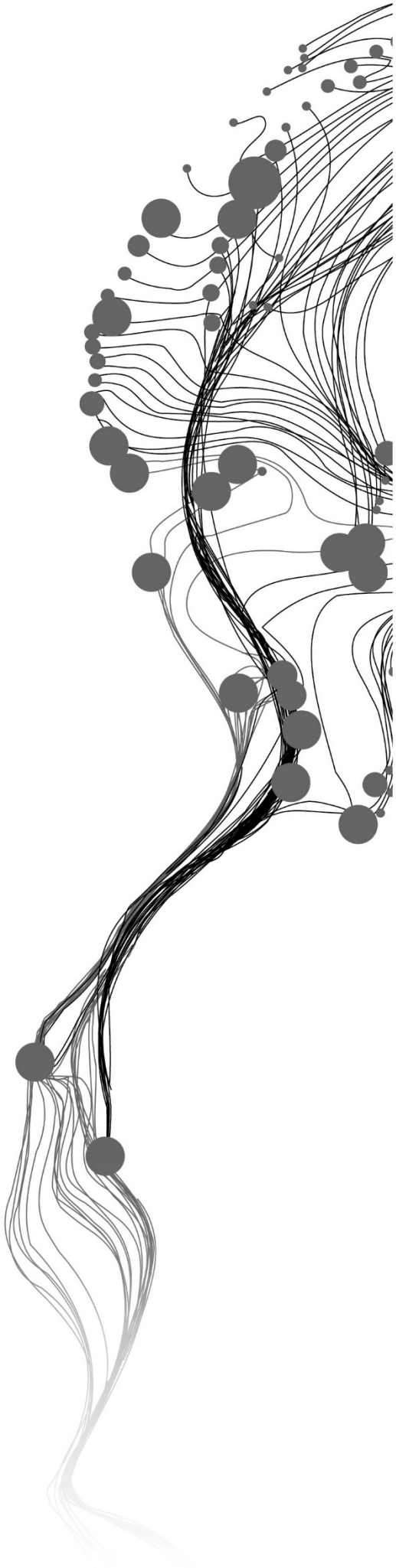

INDIVIDUAL TREE DELINEATION FROM HIGH RESOLUTION SAR IMAGE USING THE SCALE-SPACE BLOB METHOD

SEPIDEH KIA
Enschede, The Netherlands, February 2019

Thesis submitted to the Faculty of Geo-Information Science and Earth Observation of the University of Twente in partial fulfilment of the requirements for the degree of Master of Science in Geo-information Science and Earth Observation.
Specialization: Geoinformatics

SUPERVISORS:
Dr. V. Tolpekin
Dr. Y. Hussin

THESIS ASSESSMENT BOARD:
Prof. dr. A. Stein (Chair)
Dr. M. Mahour (External Examiner, Digireg B.V., Rotterdam)

ABSTRACT

Trees in the forest comprise a significant component of an ecosystem that effects the environment, and human life. However, trees outside forest also play an important role in ecological functions. In recent years, there has been high demand from different stakeholders such as environmentalists, authorities, and foresters in acquiring tree inventories. Traditionally, individual tree identification is conducted through sampling or visual interpretation of aerial photography. Nowadays, remotely sensed data such as very high spatial resolution satellite images can provide fast, accurate, and detailed information of trees, even over large areas. However, using satellite images is challenging due to the first, irregularity of tree crown projected area; second, poor separability between tree crown and similar background. This research investigates the identification of tree crown projected area from high spatial resolution, airborne synthetic aperture radar (SAR) system.

The SAR system can provide reliable and detailed information on spectral and geometrical properties of an individual tree. The spatial profile of tree crown in this study was modelled by a bell-shaped curve model. The difference between tree crown spatial profile which is affected by speckle and irregularity of tree crown with bell-shaped profile considered as noise. The smoothing property of the scale-space method allowed to successfully remove this noise. Identification of trees from gray level image due to the effect of sun illumination angle is challenging. The shadow problem has solved by using Pauli decomposition of SAR data.

In this research the main focus was on extracting this information by using the Gaussian scale-space blob method which is proper for tree delineation as an object that occurs naturally at different scales. According to this method a stack of images with successively removing image structures by increasing scale from fine to coarse can be derived. The behaviour of tree crown polygon over different levels of scale can be analytically described. In the present study, the scale parameter is equally treated with space and gray-level value. Therefore, the scale-space representation contains the feature information explicitly over scale and relation between them. Blob is defined as a significant feature which is stand out significantly in the gray-level image. To be specific the definition is referred to a region is either significantly brighter or darker than background and neighbourhood. The significant blob can be select out of many blobs which are produced by other scale-space detectors.

The Accuracy assessment is conducted using manual delineation of same high-resolution airborne SAR data. Three detection, extensional, and position uncertainty assessment show that the scale-space blob method in comparison to formal scale-space method provide accurate detection and approximation of tree crown. The study concludes that the proposed approach can be used for individual tree detection from SAR data. The obtained information from this method can be used by different stakeholders for different environmental issues such as biomass estimation.

Keywords: individual tree detection, individual tree delineation, scale-space, SAR, multi-scale method, feature detection, blob detection, gray-level image

ACKNOWLEDGEMENTS

My sincere thanks to my dear parents and my brother for their love, unfailing support and continuous encouragement and financial supporting throughout my MSc program at Faculty of Geo-Information Science and Earth Observation, University of Twente (ITC).
I would like to express my deep gratitude to Dr. Valentyn Tolpekin and Dr. Yousif Hussin, my research supervisors, for their patient guidance, continuous support, and enthusiastic encouragement.
I would like to express my great appreciation to Prof Alfred Stein, Prof Andy Nelson, Dr. Raymond Nijmeijer and Dr. Wan Bakx for their academic and motivation support.
Lastly, I would like to offer my special thanks to ITC student affairs and all ITC people.

TABLE OF CONTENTS

1. Introduction 1
   1.1. Background and justification 1
   1.2. Research gap identification 3
   1.3. Research objective 7
   1.4. Research questions 8
   1.5. Thesis structure 8
2. literature review 9
   2.1. Individual tree detection from SAR images 9
   2.2. Individual tree detection from optical images 10
3. concept and methodology 13
   3.1. Data preprocessing 14
   3.2. Theoretical background and relation to previous works 18
   3.3. Validation 26
4. study AREA AND data Description 29
   4.1. Study area 29
   4.2. Remote sensing data image description 30
5. Results 32
   5.1. Scale-space blob results 32
   5.2. Raster to vector conversion 35
   5.3. Different wavelengths of F-SAR image 36
   5.4. Validation 37
6. Discussion 40
7. conclusion and further analysis 42
   7.1. Conclusion 42
   7.2. Recommendations for further analysis 42

LIST OF FIGURES

Fig. 1.1. Tree crown projected area. 2
Fig. 1.2. An individual tree at study area with poor separability between tree and background. 6
Fig. 1.3. Noise related to tree crown irregularity and speckle precense. 6
Fig. 1.4. Different kinds of tree CPA delineation errors. 7
Fig. 3.1. Methodology framework. 13
Fig. 3.2. Radiometrically calibrated F-SAR data. 15
Fig 3.3. Data distribution histogram. 16
Fig. 3.4. Pauli decomposition. 18
Fig. 3.5. Stack of images in scale-space representation. 20
Fig. 3.6. Representation of gray-level blob definition. 21
Fig. 3.7. Descriptive definitions of a gray-level blob. 22
Fig. 3.8. False detections of a tree with two sub-crowns. 23
Fig. 3.9. Scale-space blob lifetime 24
Fig. 3.10. Four possible bifurcation events in scale-space. 25
Fig. 3.11. Detection errors (false positive and false negative errors) 27
Fig. 3.12. Extensional error 27
Fig. 3.13. Agreement assessment between reference and detected tree CPA 28
Fig. 4.1. The study area of interest. 29
Fig. 4.2. Three nominated subsets. 30
Fig. 5.1. Primary results of the scale-space blob method. 33
Fig. 5.2. Linking between gray-level blobs. 34
Fig. 5.3. Support region of significant blob related to tree CPA. 35
Fig. 5.4. Subset 3, L-band 36
Fig. 5.5. Subset3, S-band 36
Fig. 5.6. subset3, C-band 36
Fig. 5.7. Subset3 X-band. 37
Fig. 5.8. Comparision of tree CPA detection from $det\mathcal{H}L$ 37
Fig. 5.9. False negative detection of adjacent treese. 38

LIST OF TABLES

Table 3.1. Scale factor depends on the product and radiometric calibration type 14
Table 4.4.1 Characteristics of airborne F-SAR images 31
Table 5.1. Tree CPA extensional accuracy. 38
Table 5.2. Tree CPA positional accuracy 39

ACRONYMS

AFI	Area fit index
BA	Basal area
CPA	Crown projected area
DBH	Diameter at breast height
DLR	German Aerospace Centre
DSM	Digital surface model
ENL	Equivalent number of looks
GEOBIA	Geographic object-based image analysis
GIS	Geographic information system
GPS	Global positioning system
InSAR	Interferometric SAR
LiDAR	Light detection and ranging
NDVI	Normalized vegetation index
RCS	Radar cross section
RMS	Root mean square
RS	Remote sensing
RVI	Radar vegetation index
UAV	Unmanned aerial vehicle
UAVSAR	Uninhabited aerial vehicle synthetic aperture radar
VHR	Very high spatial resolution

1. INTRODUCTION

1.1. Background and justification

Trees, mostly in forest, are an essential component of an ecosystem that affects the environment, habitat life, and human life. However, trees outside the forest are also an important component of the ecosystem because they play a prominent role in the food security[1], and ecological functions such as biodiversity conservation; erosional control; air quality improvement; water protection; carbon sequestration (Dida et al., 2013). According to FAO (2002), 'trees outside forest' is defined as those trees that are neither in the forest nor in other woodland. Acquisition of inventories of these trees is a key variable in the assessment of the applications mentioned above. Thus, in recent years there has been an increasing demand for acquiring trees inventories from different stakeholders, such as environmentalists, city planners, urban authorities, foresters, and farmers. Stakeholders need detailed and up to date information for promoting sustainable tree management. Yadav et al. (2017) are referred sustainable tree management to a system that: maintains tree population; promotes biodiversity; conserves trees; removes dangerous or hazards trees; establishes tree inventory with age and species classification; just to name a few.

One of the purposes of sustainable forest management activities is related to global warming which is the increase in greenhouse gases emission. Trees can reduce this increasing emission and improve air quality. Trees can reduce this increasing emission and improve air quality. Trees are sequestering carbon dioxide (CO_2) as one of their major input, for photosynthesis purpose and even giving more oxygen (O_2) to the atmosphere. Carbon sequestration is estimated by mapping the carbon stock of trees and monitoring their variation over time (Koch, 2010). Mapping trees carbon stock can be fulfilled based upon their biomass[2] estimation (Vashum & Jayakumar, 2012). Estimating tree's biomass provides a reliable perspective of their potential in carbon store and sequestration within the ecosystem. Therefore, to accomplish accurate modeling of biomass estimation there is a great demand for tree measurements which are accurate and up to date.

A tree, within a group or standing individually, may have different spatial patterns and characteristics. To assess their patterns and characteristics, various geometrical and physical parameters such as location, diameter at breast height (DBH), basal area (BA), height, crown size, and species identification are used (Gomes & Maillard, 2016). Among these variables, tree crown size is a prominent variable since it is significantly correlated with the growth of the tree (Lin et al., 2017). Based on an existing definition's review, for consistent reporting, common tree related definitions are required. In addition in line with the focus of present research, to improve the fitting precision and prediction accuracy of the whole tree biomass model, introduction of the tree crown projection area for each tree can be efficient (Zhang et al., 2011). Throughout this study, the crown projected area (CPA) as shown in Fig. 1.1 refers to vertically projecting the crown primitive (Gschwantner et al., 2009). From tree CPA measurement, it is possible to derive the size of the tree crown followed by its position. In addition, tree crown shape can be described by different mathematical models such as Pollock, Gaussian, and Paraboloid. Ramezani (2015) identified tree species based on Pollock parameters. Moreover, according to prior studies, CPA is highly correlated

[1] Trees have important role in insurance of the provision of ecosystem services to the sustainable agriculture system.

[2] Biomass definition gives by all mixture of organic materials such as wood, agriculture crops or wastes, in particular which utilized as an energy source.

with height and carbon stock of tree (Zhang Li-fu et al., 2011; Paper, 2014; Mbaabu et al., 2014). Shah et al. (2011) investigated that there is a linear relationship between the CPA and the DBH of a single tree. Based on the inventories obtained from a tree CPA, various related information such as mapping structural attributes (height, basal area, biomass, volume); monitoring disturbance (logging, fire, windthrow, insect damage); monitoring photosynthetic processes (growing season length); monitoring change (deforestation, degradation, reforestation) can be derived. This information is critical to the series of activities in relevance tree management and conservative outside the forest (e.g., growth level assessment and biomass estimation). In addition, they can be useful for horticulture[3] counting and monitoring relevant damage and accident prevention.

Nowadays, trees inventory data are derived widely using different kinds of remote sensing (RS) data acquisition approaches, instead of using traditional methods such as random sampling or visual interpretation of aerial photography (USDA, 2002). Some of the recently developed RS approaches, that are used commonly for tree inventories measurement, are global positioning system (GPS), satellite images, and unmanned aerial vehicle (UAV) respectively (OpenForests.com). During recent years, by the development of these methods, obtaining information is time and cost effective. On the contrary of traditional approaches, these methods can reproduce advance information as well as detailed data of tree inventories even for large areas. Also, using remotely sensed data acquisition approaches can be useful when a parameter measurement from a sampling method is not efficient, e.g., tree crown boundary measurement (Schmitt et al., 2015). In other words, the main advantage of these approaches in regard to the topic of this study is providing up-to-date information and a synoptic view over large areas, since some of the forest inventories change rapidly. Therefore, RS data sources provide reliable and detailed information with sufficient spectral and geometrical details which is the most appropriate data source to delineate and detect individual tree CPA boundary. In this way, an automated individual tree detection algorithm relates tree counting, and tree delineation corresponds to defining a position and tree crown boundary.

Although using RS data sources is an efficient way of deriving detailed information and advanced knowledge, the tree is a complex object in terms of retrieving crown projected area (Ardila et al., 2012). As it appears from Fig. 1.1 extracting tree crown boundary from images is challenging due to the tree crown irregularity. To recognise tree CPA, a wide range of automatic and semi-automatic image analysis methods is available, especially from passive remotely sensed images (Ardila, 2012). To highlight the progress in image analysis, a comprehensive review of previously introduced methods and data sources is discussed in the following section.

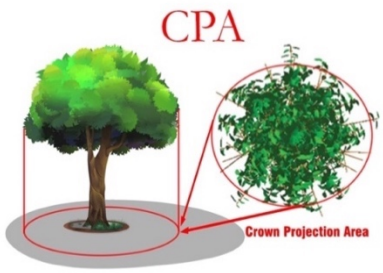

Fig. 1.1. This figure provides front view and top view of a tree with shadow (gray circle) at left and at the right, respectively. We tried to model the tree crown boundary by the red line. However, obviously tree crown is a complex spatial object to fit a model. Source: (Adopted from lecture slides, 2018 y.a.hussin@utwente.nl).

[3] Horticulture is the science or art of fruits, vegetables, flowers, or ornamental plants cultivation include orchards.

1.2. Research gap identification

This research is undertaken to identify the CPA of individual trees outside the forest from a very high spatial resolution (VHR) airborne F-SAR images. To be specific, it appears from previous studies that the spatial resolution of optical satellite images from different perspectives is primary concern in individual tree crown identification. Mapping tree CPA from different spatial resolution RS images has been dealing with various limitations. One of the main limitations is relating to vision[4] definition of tree CPA boundary since the tree crown boundary only exists as a meaningful object over a limited range of scales. For example, branches and leaves of an individual tree may be discernible in the VHR remotely sensed data, whereas it is not simple to group them correctly to recognise a tree crown. Tree crowns may have merged at a coarser scale level of RS data with its neighbors, or even they are not detectable due to the limited spatial resolution of images in relevant tree size on the ground. Therefore, in one hand a method which can provide a multiresolution representation of the tree CPA in an image is crucial. On the other hand, most of the researchers have addressed VHR optical remotely sensed data as an appropriate data source; however, still, there are some deficiencies. Ardila (2012) mentioned some of the main constraining issues of VHR images concerning individual tree CPA detection, despite the fact that optical VHR images can provide efficient spectral and geometrical information. One of the major limitations of the VHR passive satellite images as depicted from Fig. 1.2, is that the spectral separability between tree crown canopies with large variance and other similar background classes (e.g., grasses and shrubs), is poor (Tolpekin et al., 2010). In addition, tree crown size variation brings the difficulty of analysis whereby an individually detected tree may represent a separate branch or group of trees (Pu & Landry, 2012). In this way, for the purpose of tree CPA boundary detection and delineation, noise can be defined as the excessive precision of the tree crown boundary shape. Therefore, high spatial resolution images contain more noise due to the irregular canopy profile; see Fig. 1.3. The predominant difference between spatial profile line of tree crown and Gaussian function line illustrates this noise and effect of speckle in high-resolution SAR image. As another example of popular data source, Khosravipour (2017) detected individual trees from light detection and ranging (LiDAR). Tree identification from LiDAR dataset provides tree height information explicitly. Thus, the problem of poor spectral separability with the background can be covered. In principle, the contrast between spectral bands of converted LiDAR point cloud to raster, especially for similar background vegetation type is low. However, the contrast in height of tree and background is substantial. The main problem of this dataset is high costs for trees outside the forest and large areas. Moreover, the accuracy of results depends on the quality of the digital surface model (DSM). Another source of experimental limitations is corresponding to a tree located under other trees, different sun illumination angle, or tree in the shade (Wulder et al., 2000).

Several automatic and semi-automatic image analysis methods such as local maxima, valley following, watershed, region-based image segmentation, and even hybrid algorithms[5] have been developed to identify individual tree CPA from VHR images (Gomes & Maillard, 2016). These approaches attempt to recognise tree CPA with high precision and restrict the limitations of individual tree CPA recognition from VHR optical satellite images. However, the proposed methods did not cover all the restrictions of mapping individual tree CPA from VHR passive satellite images. Ardila et al. (2012b) developed a geographic object-based image analysis (GEOBIA) [6] method to address the problems of single tree crowns identification from VHR optical images. The study via integration of several methodology's results aimed

[4] Vision is defined as the process of discovering what is present in the world, and where is it (Marr, 1982).

[5] One algorithm for tree crown detection and another for tree crown delineation.

[6] Contained several methods such as multi-scale segmentation, local contrast segmentation, analysis of tree shadow, local maxima filtering, morphological object reshaping and region growing.

to extract all the spatial, spectral and contextual characteristics of trees. This study showed the capability of remotely sensed data in extracting detailed information on tree inventories. However, the attempt dealt with ample limitations related to the spatial resolution of images, adjacent tree interlock, and low contrast between trees and background. These restrictions correspond to some over- and under-identification errors. Consequently, the study recognised that may be a multi-scale approach is appropriate for tree CPA delineation in urban areas. In other words, all previous methods for tree crown boundary detection have referenced to a specific resolution and, they do not easily translate from one scale to another scale. However, with the use of UAV, uninhabited aerial vehicle synthetic aperture radar (UAVSAR), or some other satellite images, there is a possibility to obtain an image of various resolution. Moreover, identifying a tree crown boundary from satellite images can be done with segmentation methods. Tree crown boundary can be distorted by the wind; therefore, it may not be an accurate estimate of a geometrical parameter that can be correlated with other parameters of the tree for different applications.

Brandtberg & Walter (1998) proposed a multiple-scale algorithm for automatic delineation of deciduous trees CPA from high spatial resolution infrared colour aerial images. They used an edge segment to describe a model of tree crown boundary region. The main problem of this algorithm was the necessity of prior knowledge about tree diameter to find an optimal window size of individual trees for low pass filter in the image. As a result, Brandtberg (2002) proposed to use the scale-space method to solve the problem. The scale-space method is a well-founded mathematical framework that generates a multi-scale representation of an original image. The scale-space representation at "zero scale" is equal to the original image, and by increasing scale, the representation is the convolution of the original image with two-dimensional Gaussian kernel (Lindeberg & Eklundh, 1991). The underlying assumption of using the scale-space approach for identification of tree CPA is that tree crown distribution has an approximately bell-shaped intensity profile in the normalized vegetation index (NDVI) image (Ardila, 2012). Effect of NDVI on an image is mainly used to remove the shadow of trees on the ground. Mahour et al. (2016) used the scale-space method to detect two orchard tree types with different sizes from VHR remote sensing images. Thus, this study demonstrated the capability of the scale-space combined with blob-feature detection methods for individual tree CPA identification with accuracy higher than 80%. However, the study focused just on VHR images and faced with some detection problems, such as an overlapping circular object detected from a single tree, inaccurate tree size measurement, and lack of identification of small trees.

Further investigation of using the scale-space methods for tree detection from VHR images carried out by Mahour et al. (2018). In this study, the automatic Gaussian scale-space model of individual tree detection and delineation from passive VHR images is improved. In the scale direction, two empirical models of the tree are introduced and computed to provide better tree descriptor and more accurate tree size estimation. Although the study increased the accuracy of the true tree detection from false detections, still some overestimation and underestimation problems have remained. The main deficiencies are referred to as false positive and false negative detections (e.g., false detection of trees with two or more sub crowns). In addition, the accuracy of tree size and position, and the identification of precise tree crown boundary are needs to address (Fig. 1.4). The information related to tree crown recognition in the proposed scale-space algorithms until now is implicit, means not computed. Feature is referred to interesting part of an image which needs to identify. The features or relation between features should be represented explicitly over different levels of scale to correspond to main features at the original image. Lindeberg & Eklundh (1991) called this method scale-space blob method. By using the suggested algorithm in the present study aims at obtaining features; i.e. tree crowns, which are significant in scale-space. The underlying assumption is that

scale-space features with high scale-space volume in scale-space associated with relevant objects in the image. This algorithm can be performed by making features as well as their relationship in scale-space representation explicit over a scale. By adding fourth dimensional gray-level landscape, predominant areas[7] in the image will be described by spatial and the gray-level values in the specific range of scale. Thus, the significance of the spatial features between different scale levels will be compared and the representation will reflect the shape of gray-level features. There will be no need for any external criteria or tuning parameters in the selection of proper scale.

Generally, all attempts for identification of individual trees has been widely investigated either on passive VHR images or active LiDAR images. However, active or passive VHR images are not always available, or often they are costly, especially for the identification of trees outside the forest at large areas. On the other hand, based on best of author knowledge and extensive literature review, studies on synthetic aperture radar (SAR) are relatively limited. It is due to the coarse spatial resolution of available SAR images, whereas SAR is providing true measurements of the scattering properties of the Earth's surface (Oliver & Quegan, 2004). Recently high-resolution SAR systems are getting an upsurge of attention due to the different capabilities such as estimation of forest biomass and volume using L wavelength tomography (Mercer et al., 2010; Neumann et al., 2010), or reconstruction of canopy height model using X wavelength interferometry (Izzawati et al., 2006). Schmitt et al. (2013, 2015b) have been investigated the potential of airborne interferometric SAR (InSAR[8]) datasets in individual tree recognition. Because of the different looking angle property of the SAR system, it can provide more accurate position information of single tree CPA measurement. Moreover, in addition to horizontal CPA information which is provided by optical RS data, SAR data can provide horizontal and vertical information (i.e. tree boundary height or treetop height) simultaneously (Varekamp, 2001). However, identifying tree CPA from SAR images is challenging as well. The results of individual tree recognition from InSAR image is affected by shadow and two types of shifts in sensor direction, i.e., in intensity maxima and tree height. In addition, all kinds of SAR data are suffering from the presence of speckle and even fully developed speckle in coarse resolution SAR images. Speckle is a multiplicative noise-like phenomenon which is present in the SAR images due to the coherent interference of the backscatters within per resolution cell. Fully developed speckle occurs in coarse resolution SAR where several random distributed scatters are present within a resolution cell (Lee & Pottier, 2009). Since the scale-space representation is the result of convolution of the image with Gaussian kernel, we assume that it can deal and reduce the effect of speckle, and additive noise of F-SAR images.

Therefore, the significance of these two gaps motivated the author to investigate the capability of the scale-space blob methods in the identification of tree CPA boundaries from high airborne F-SAR data. The general idea is an implementation of scale-space methods in extracting detailed information of an object in the different range of scale from SAR images, which have not been explored. To reach this goal, this study will use high spatial resolution airborne F-SAR images.

[7] These areas will be named further blob.

[8] Using difference in phase information to extract digital elevation model.

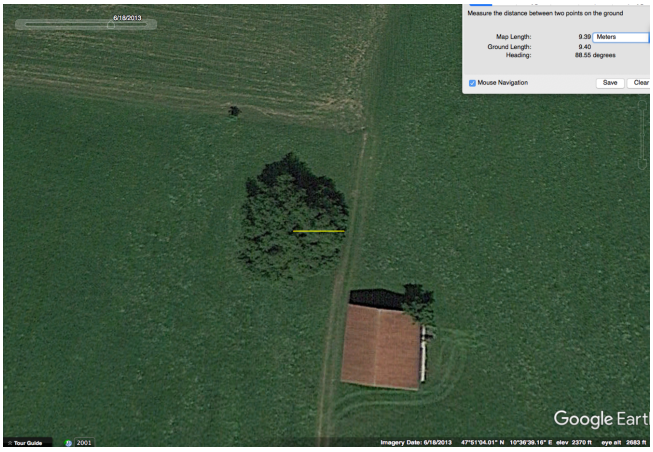

Fig. 1.2. An individual tree at study area with diameter information at the right top. The image demonstrates poor separability between tree and background (source: GoogleEarth).

a)

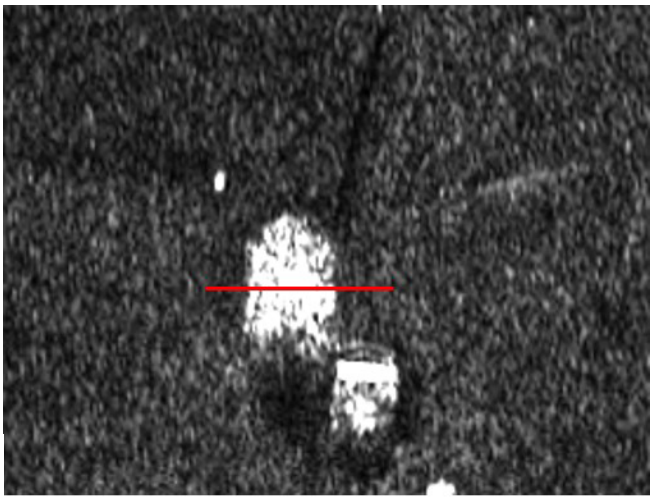

b)

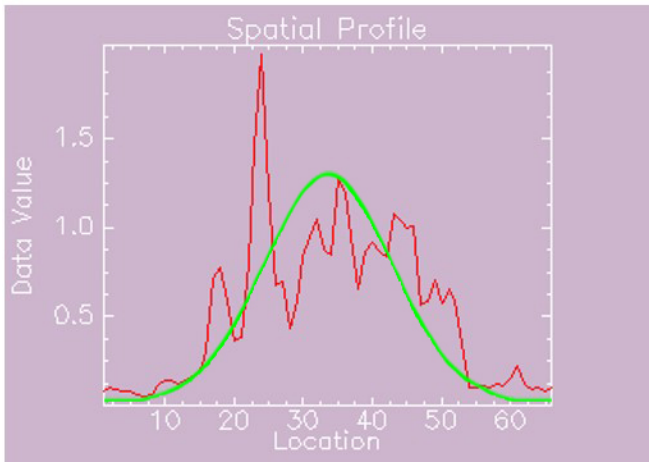

Fig. 1.3. a) Amplitude F-SAR image of L-band, polarization HH. The red line is a transect profile line (true signal component). b) Red line is the spatial profile of tree crown, and the green line is Gaussian function. The difference between two lines caused by noise which is related to the irregularity of tree crown object and effect of speckle.

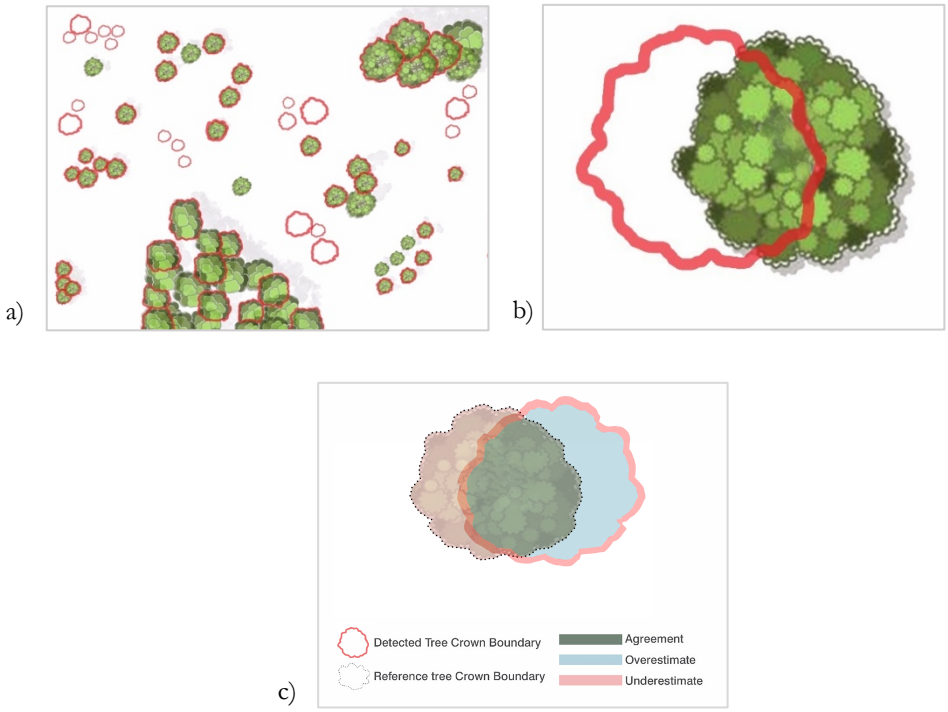

Fig. 1.4. Denotes different kinds of tree CPA delineation errors a) Different kinds of detection errors (false positive and false negative), b) Positional error, c) Extensional error

1.3. Research objective

This section is illustrating the main objective of this research which follows by specific objectives related to data sources and the used method. To be more specific, the most controversial questions to solve specific objectives entirely are figured out.

1.3.1. General objective

The main objective of this research is:
To explore and perform individual tree detection outside of the forest from airborne F-SAR images by applying scale-space methods.

1.3.2. Specific objectives

1. To generate the multi-scale representation of blobs which are correspond to individual tree CPA at all scale levels.
2. To determine the significant blob in scale-space representation and extract the tree CPA boundary based on the spatial extent of the gray-level blob.
3. To investigate how well the true signal component related to the tree can be separated from the noise and speckle.
4. To compare the result of scale-space blob method and the combined scale-space method with the differential interest point detector in scale-space and random sets methods.
5. To explore the possibility of using the scale-space methods on high-resolution SAR images with different wavelengths for identifying tree crown.
6. To determine the accuracy of individual tree delineation from F-SAR images results by applying scale-space blob methods.

1.4. Research questions

1. How to generate the multi-scale representation of gray-level image?
2. How different properties of the scale-space blob can affect the accuracy of detection and delineation of tree crown boundary?
3. Does the smoothing property of the scale-space methods suppress the noise and speckle?
4. How different wavelengths of SAR images affect the results of tree detection?
5. Which kind of information can be obtained from different wavelengths of FSAR images?
6. What is the probability distribution function of speckle in fine resolution SAR image?
7. How accurate can be individual tree crown boundary detection and delineation from FSAR images?
8. How well the Gaussian filter works for SAR data in case of fully developed speckle in asymmetrically distributed (exponential or Rayleigh distribution) single look SAR image?

1.5. Thesis structure

The thesis is structured into below main chapters:

- Chapter 2 review previous attempt for individual tree detection based on two main type of data sources.
- Chapter3 implies concept and methodology includes data preprocessing steps and the. implemented method and the uncertainty assessment.
- Chapter 4 briefly describes the study area and characteristics of provided data for this research.
- Chapter 5 provides the results gained in this study.
- Chapter 6 discuss the results to provide an appropriate interpretation of them.
- Chapter 7 ends this study by providing the conclusion and recommendations for further investigations.

2. LITERATURE REVIEW

Trees are playing a fundamental role in the environment and human life. Researchers have introduced and developed plenty of methodologies to identify trees generally from VHR satellite images. This chapter gives an overview of previous different methods that have applied on different satellite images to identify individual trees outside the forest. The choice of a spatial resolution of the RS data source to identify tree CPA has been a controversial issue since it restricted to several factors, e.g. the size of a tree, a spatial resolution of an image, cost of data source, spectral and temporal characteristics of an image. Thus, the chapter is divided into two sections: first, the image analysis methods have applied on two main data sources (i.e. SAR and optical), second, different multi-scale methods. In the end, summarization of the method which constitutes the main concept of the present study is provided.

2.1. Individual tree detection from SAR images

In the last few years, a variety of spaceborne and airborne SAR images with different quality[9] have been produced. In principle, SAR systems measure the local interaction between an incident wave and the Earth (Oliver & Quegan, 2004). SAR provides multidimensional measurements of scattering properties of the Earth, i.e. surface scattering from top of the canopy, volume scattering, surface and volume scattering from the ground. Variety of product can be formed from the SAR data which known as 'complex image' based on an application at hand. For instance, the amplitude A, the phase φ, the intensity[10] I (i.e. $I = A^2$), and the logarithm base 10 intensity $\log \mathrm{I}$. In working with all kinds of SAR products, must take account of coherent speckle for all measurements or inferences, as an inherent property. Speckle is a multiplicative noiselike[11] phenomenon which happens in case of interference between many discrete backscatters within per resolution cell. Finding an appropriate image processing method to convert the electromagnetic scattering properties to application related information is what concerns a lot of researchers (Oliver & Quegan, 2004). Section 4 concerned about speckle distribution of airborne FSAR and Sentinel-1 images, and how the scale-space method can deal with it.

There is a large volume of published studies throughout the world using different SAR data on forest mapping and monitoring, extracting tree volume, forest biomass, forest structure and type, forest fire, thermal state, and to name a few (Balzter, 2001; Heiko Balzter et al., 2007; Vashum & Jayakumar, 2012; Tanase & Aponte, 2015). As an example, Olesk et al. (2016) focused on developing semi-empirical models for forest height estimation by using a combination of temporal single polarimetric InSAR and LiDAR data.

In the scale of an individual tree, Loong et al. (2013) co-registered two single scatter SAR images of the same area in sub-pixel level to extract height of oil palm tree via using phase information. However, only recently two papers have investigated the potential of airborne SAR data for individual tree recognition. Schmitt, et al., (2013b) used single-pass millimeterwave InSAR data to clarify the potential of fine-

[9] Different wavelengths, and different polarimetric capabilities of SAR sensors.

[10] The word "intensity" is synonymous with power or energy.

[11] Speckle is not noise, since it is a real electromagnetic measurement and can be exploited as product such as interferometry products.

resolution airborne InSAR data (decimetre in range and azimuth resolution) for the analysis of forest areas on a single tree level. The results of the Local maxima technique with prior derived knowledge on tree height from interferometric phase information are served as a preliminary tree hypothesis. In the end, the 3D-georeferenced positions of trees in a world coordinate system are used as inputs for tree crown recognition. As a second attempt, Schmitt et al. (2015) represented an unsupervised approach to multi-aspect millimeterwave TomoSAR data for segmentation and individual tree reconstruction. Important and efficient tree parameters such as tree location, tree height, and tree crown diameter have been derived. However, he mentioned the limitation of SAR imagery due to the side-looking in detecting small trees which are surrounded by large trees.

2.2. Individual tree detection from optical images

Ample automatic and semi-automatic methods have been developed for recognition of individual tree crowns and the characteristic extraction in passive optical satellite images (Larsen et al., 2011). Local maxima, valley following, watershed segmentation and region growing are four of the most common algorithms used in individual tree identification and delineation of their spatial patterns. However, several approaches utilized hybrid methods; one algorithm for tree detection and another for delineation of tree crown, or one approach used as an initial approximation and another to fine-tune the results (Gomes & Maillard, 2016). Even in some researches more than two techniques are applied (Larsen et al., 2011). Furthermore, different tree species may have different tree crown texture and shape (e.g., conifers, broadleaves, and deciduous) which is an important factor in the implementation of different tree crown boundary delineation methods.

Local maxima is the simplest filtering technique that can be used to identifying tree crowns based on the gray level image. By scanning the entire image using a search window, the brightest gray pixel of that image is detected as the center of the tree crown boundary. Although, it shows promising results for conifers with high reflectance gray level pixel at the top of the tree. The results are susceptible to crown size variation, search window size and spatial distribution of tree. For instance, it increases commission and omission errors for small and large search windows, respectively. On the other hand, valley following is consisting of an analogy that delineating tree crowns by identifying the shaded spots between tree crowns (valleys), then the bright spots will be crowns (hills). The performance of this method is good in a combination of low solar elevation angle images and conical shape trees. However, it leads to group multiple small trees in one segment, in particular, if the trees are asymmetric with different species and crown size. Another technique similar to valley following is the watershed method which is related to defining segments based on thresholding process on gray values of the image. To prevent over-segmentation, the selection of markers which represent the tree crowns center has been implemented (Gomes & Maillard, 2016). Region growing algorithm generates segments and expands the region from seed points based on predefined criteria. The results of tree crown delineation are promising for trees with complex shapes, whereas the algorithm is too complex due to several different rules for different environments. Moreover, it is sensitive to the branch of similar trees (Larsen et al., 2011). As an example of hybrid methods, the GEOBIA method which is a combination of multi-scale segmentation, local contrast segmentation, analysis of tree shadow, local maxima filtering, morphological object reshaping and region growing is investigated by Ardila et al. (2012b). The classification rules are determined for multiple scale segmentation of trees, as an object of interest. This classification can modify the labelling and shape of trees on the image to consider all spatial, spectral, and contextual information of trees within the urban

forest[12]. The method is bias in the detection of small and adjacent overlapped trees with low contrast with the background. It resulted to false negative errors and false positive errors. In addition, the precision of method in a delineation of tree CPA boundary is not acceptable. All these studies head us to use a multi-scale approach due to the inherent definition of different tree CPA sizes on a different scale of satellite images.

[12] All individual and group of stands trees either within or close to the urban areas.

3. CONCEPT AND METHODOLOGY

The major concern of this study is establishing a viable representation of a data-driven model, in which information can be correlated to measurements and their spatial disposition without depending on any specific external parameters. The research steps contain pre-processing and method parts to reach the mentioned objectives in section 1.3 is depicted in Fig. 3.1.

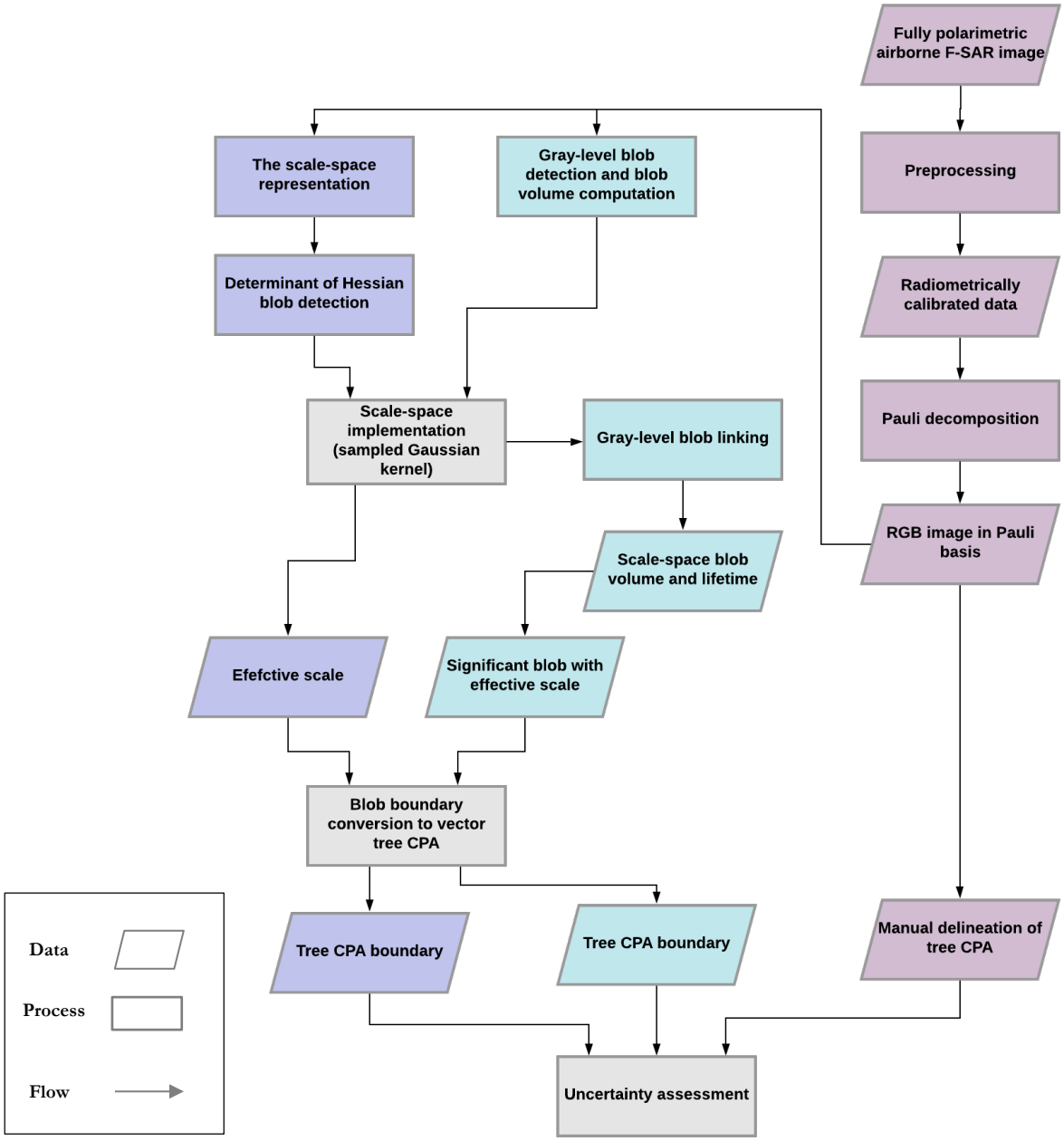

Fig. 3.1. Schematic flowchart for tree CPA detection from airborne F-SAR images by using both scale-space and scale-space blob algorithms.

3.1. Data preprocessing

3.1.1. SAR data calibration

SAR images are estimating complex backscattering at each pixel as a linear measurement system. Therefore, there are different representation images of a complex SAR data (i.e. $\mathrm{A}, \varphi, \mathrm{I}$, and $\log \mathrm{I}$). According to Oliver & Quegan (2004), an efficient radiometric calibration of these images can provide a true measurement of the scattering properties of the Earth's surface. Therefore, the available F-SAR data depends on the research purpose can be radiometrically corrected based on β_0, σ_0, or γ_0 (Keller et al., 2016). σ_0, which known as radar cross section (RCS) or backscattering coefficient is the measure of the target's reflectivity in direction of radar receiver (Nicolaescu & Oroian, 2001). In the lack of any prior knowledge or assumption about the target's reflectivity, σ^0 can be estimated based on the intensity image. The average of intensity measurements[13] gives the best estimation of σ^0. This process of intensity averaging is known as 'multilooking'. In addition, in calibrated data, each pixel correlated with estimation of the backscattering coefficient σ^0 in dB, which is linearly scaled (Oliver & Quegan, 2004). The "dB" image known as log transformed image or log image. The F-SAR image can be unity scaled to dB values for any type of the calibration by taking below formula (taking $10\log_{10}$ of each pixel intensity):

$$I_{dB} = 10 \log \left(\langle f |I_{in}|^2 \rangle\right),$$

where I_{in} is the input image, the meaning of multi-looking or spatial averaging is defined by $\langle . \rangle$, and $|.|$ denotes the matrix norm of the intensity image. $f: \mathbb{R} \rightarrow \mathbb{R}$ stands for the scale factor which has been selected based on the product and radiometric calibration type (Table 3.1).

Table 3.1. Scale factor depends on the product and radiometric calibration type

Input image	Product type	Scale factor (f)		
		β_0	σ_0	γ_0
slc	RGI-SR, INF-SR	1	$\sin(\theta_{inc})$	$\tan(\theta_{inc})$
amp	RGI-SR, GTC-IMG	$1/\tan(\theta_{inc})$	$\cos(\theta_{inc})$	1

The amplitude image from GTC-IMG product is used to compute σ^0. The airborne F-SAR images includes all HH, HV, VH, and VV polarisation for all wavelengths. This kind of SAR images is called full polarised. The radiometric calibration computation is repeated for all different full polarised wavelengths. As an example, the results of the L band of subset 3 is shown at Fig. 3.2. Throughout this research, RCS is referred to as the mean intensity (σ), since the data is properly calibrated.

[13] Called "incoherent averaging" since phase information is discarded.

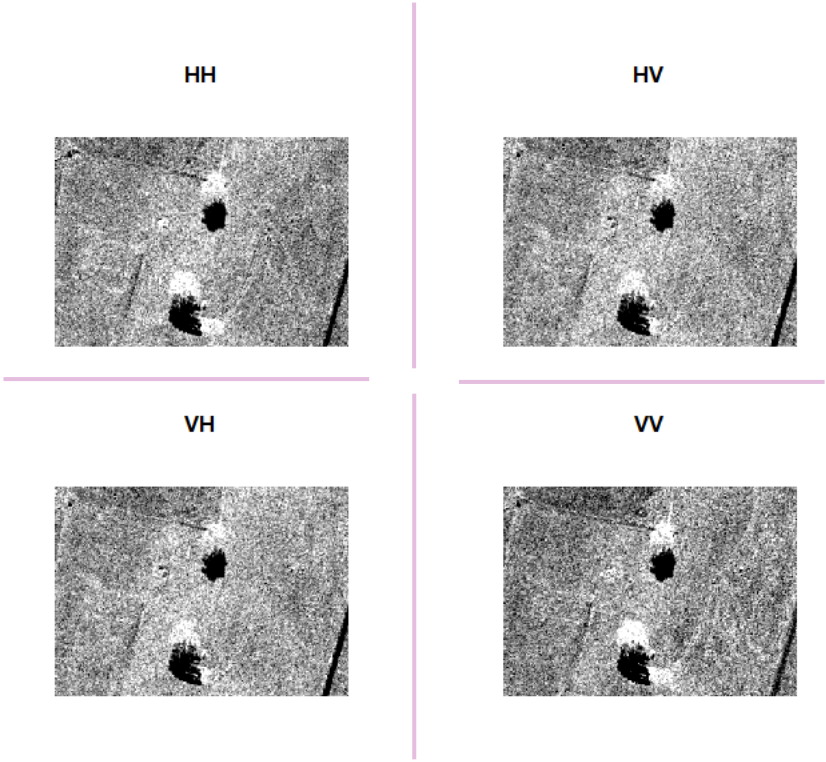

Fig. 3.2. Radiometrically calibrated representation of the fully polarized amplitude image of L-band, subset 3.

3.1.2. Speckle distribution

To describe the original data distribution and also the smoothing effects of radiometric calibration as well as Gaussian scale-space, the "equivalent number of looks" (ENL) is applied. The ENL is the number of averaged intensity values per pixel (Anfinsen et al, 2009). The below equation is carried out ENL over a small and homogenous subset of intensity,

$$\mathrm{ENL} = \frac{(\mathrm{mean})^2}{\mathrm{variance}} \tag{3.1}$$

It is applied mostly to describe the properties of the original data[14]. For display purpose, to reduce dynamic range $A = \sqrt{I}$ is preferred. The L-look data generally have 'square root gamma distribution'

$$P_A(A) = \frac{2}{\Gamma(L)} \left(\frac{L}{\sigma}\right)^L A^{2L-1} e^{-LA^2/\sigma} \qquad A \geq 0. \tag{3.2}$$

In 3.1, $P_A(A)$ is the probability distribution of amplitude image, L in this equation is equal to ENL, and as mentioned before σ is referred to RCS. The model of the intensity distribution of SAR data with more than one look assume to have a gamma distribution function (Oliver & Quegan, 2004). On the other hand, speckle noise is appearing in the SAR images due to the coherent interference of the backscatters

[14] It is not necessarily integer number.

(Lee & Pottier, 2009). Fully developed speckle occurs in coarse resolution SAR where several random distributed scatters are present within a resolution cell, when the range distance is larger than the radar wavelength (Lee & Pottier, 2009). In contrast, speckle in fine spatial resolution SAR is not fully developed and has different characteristics from speckle in coarser spatial resolution SAR images.

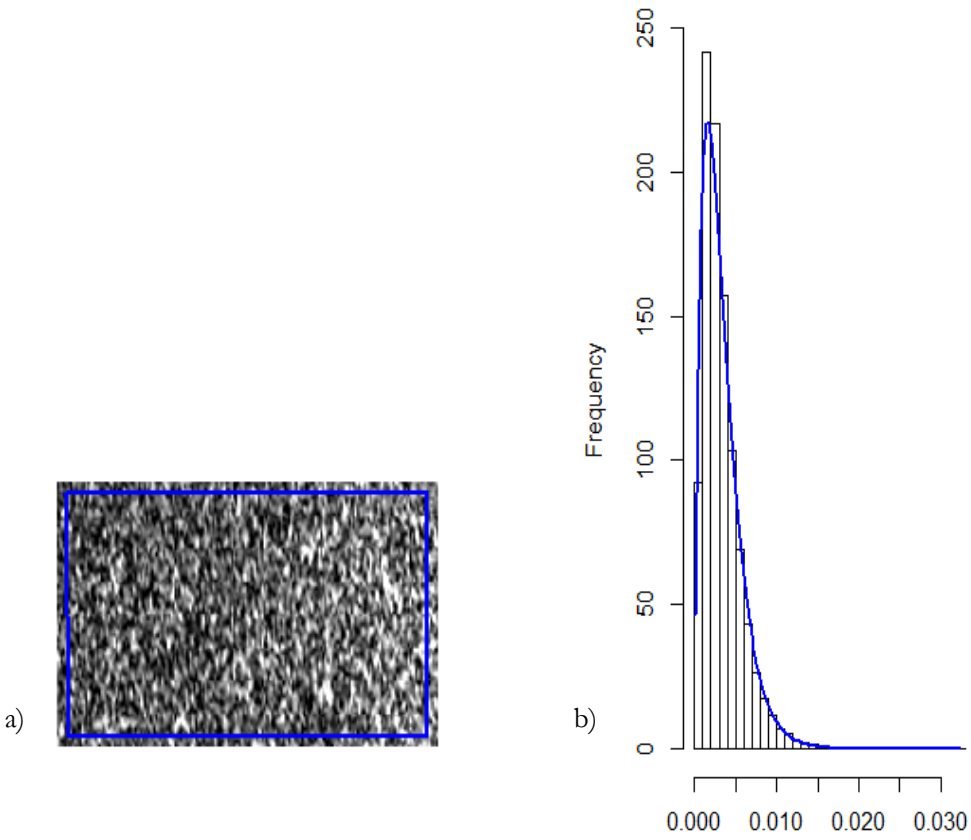

Fig 3.3. a) intensity image, L band, polarisation HH b) two-look gamma distribution with histogram.

To determine the speckle distribution of SAR data, small homogeneous subsets from different polarization of L, X, S, and C bands amplitude images are extracted. The intensity image obtained based on the amplitude images. Here only the probability distribution of a polarization HH of L-band is presented. According to Oliver & Quegan (2004) and as presented in Fig 3.3, the F-SAR image has a gamma probability distribution[15] function.

3.1.3. Pauli decomposition

To retrieve information about the target, transmitted and backscattered wave information which is described in the scattering matrix (equation 3.1) can be used (Sakshaug, 2013).

[15] Gamma distribution is family of probability distributions with two-parameter such as exponential distribution.

$$S = \begin{pmatrix} S_{hh} & S_{hv} \\ S_{vh} & S_{vv} \end{pmatrix} \tag{3.3}$$

In this research, it has been assumed that $S_{hv} = S_{vh}$, as in monostatic system[16] reciprocity performs. Thus, the reformed scattering matrix for pixel i is $S_i = [S_{hh} \quad \sqrt{2}S_{hv} \quad S_{vv}]^T$. In addition, via appropriate statistic characterization, the difference between log transformed HV and VH is calculated. Fig. 3.4 presents this difference which can also show the strength of noise in this data. In addition, this histogram indicates that the data is properly calibrated. The standard deviation is equal to 0.001563282 with the mean of 7.977679e-05.

According to Sakshaug (2013), representation of all the polarimetric information of F-SAR image can be employed via the Pauli decomposition of the scattering matrix in a single RGB image (Fig. 3.4). The Pauli basis expresses the measured scattering matrix as a linear combination of three scattering mechanism

$$S_{2\times2} = \alpha \begin{bmatrix} 1 & 0 \\ 0 & 1 \end{bmatrix} + \beta \begin{bmatrix} 1 & 0 \\ 0 & -1 \end{bmatrix} + \gamma \begin{bmatrix} 0 & 1 \\ 1 & 0 \end{bmatrix} \tag{3.4}$$

Where

$$\alpha = \frac{S_{hh} + S_{vv}}{\sqrt{2}}, \beta = \frac{S_{hh} - S_{vv}}{\sqrt{2}}, \gamma = \sqrt{2}S_{hv} \tag{3.5}$$

The interpretation of the RGB image in Fig. 3.4 can be described based on a value for each of the coefficients per pixel as below (Lee et al, 2004):

- The sea appears blue on the RGB image. So, the magnitude of first polarimetric channel $|HH + VV|$, is large in comparison to other channels, i.e. the HV amplitude is weak and the $HHVV^*$ phase argument is almost zero. This channel indicates the odd or single bounce scatters which is characteristics of surface scattering.

- The white and red are dominant colors over the buildup areas, vehicle, and man-made objects. Between all polarimetric channels, equal amplitudes appear in white, whereas red pixels correspond to π for $HHVV^*$ phase argument. They are depicting double or even bounce scattering.

- The green color denotes forested area, i.e. wave reflection from a canopy. The HV component would be dominant, and it would be interpreted as volume scattering.

[16] In monostatic radar system, transmitter and receiver stations are sharing a common antenna. So, it will generate three bands instead of four bands.

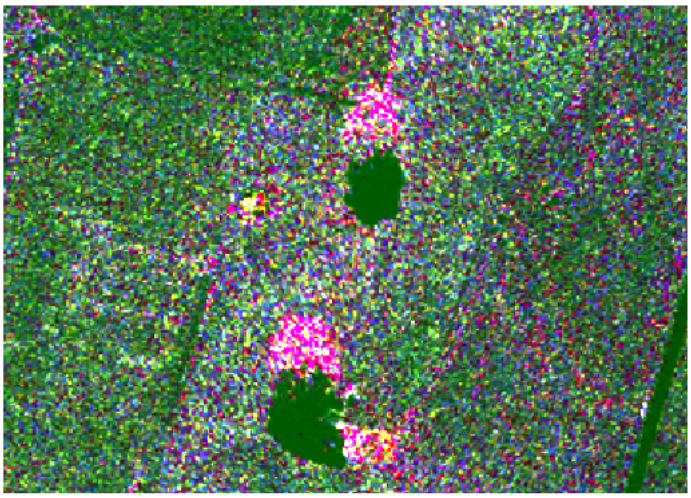

Fig. 3.4. Pauli decompositions of subset3, X-band. The resulting coefficients $\alpha, \beta,$ and γ are associated to the blue, red and green colors in the image respectively.

Although in the research done by Mahour et al, (2016) on VHR optical images the shadow effect removed by applying NDVI but applying radar vegetation index (RVI) on F-Sar image to reach same purpose did not respond. Thus, as it is apparent from Fig. 3.4, the main advantages of using the Pauli decomposition for this research is removing the shadow.

3.2. Theoretical background and relation to previous works

An inherent property of some features is that they are only meaningful over a certain range of scale. For instance, the tree crown object as discussed in the introduction chapter only exists and detectable on a certain resolution of satellite images. They are not detectable from coarse resolution images due to the small tree size in comparison pixel size. Therefore, considering the vision phenomenon of tree crown detection from satellite images, including the notion of scale in an image analysis approach is necessary.

Brandtberg & Walter (1998) presented a multi-scale method to recognise deciduous trees crown from VHR infrared colour aerial images. They used an edge segmentation algorithm at the current scale to describe a model of tree crown boundary region. The transformation of scale done based on scale interval significance value. The main problem of this algorithm was the necessity of prior knowledge about tree diameter to find an optimal window size of individual trees for low pass filter in the image. As a result, Brandtberg (2002) proposed to use the scale-space method which does not need any prior knowledge. The scale-space representation of an image in computer vision, proposed by Lindeberg (1994).

Scale-space methods are a bottom-up multi-resolution representation framework, to deal with features such as tree crowns which occur at the different level of scales. Scale-space treats scale parameter continuously as well as other parameters of images which allow to 'select' an image at any resolution. By increasing scale from fine to coarse, the resolution of the image will decrease and blurred, whereas spatial sampling such as a number of pixels at all scales is remained the same. On the contrary of other multi-scale approaches, scale-space is based on precise mathematical definitions of tree model, which can be

illustrated analytically over different scales. This applied for individual tree detection first from VHR colour infrared aerial photographs by Brandtberg (2002), then from VHR satellite image by Mahour et al., (2016). Mahour et al., (2016) detected two types of orchard trees, i.e., walnut and peach, from worldwide-2 image.

The purpose of the present research is complementing previous works first by indicating the capability of scale-space methods in feature detection without using any external criteria; second, investigating the scale-space methods in tree CPA detection and delineation, as an object of interest, from airborne F-SAR image. The complementation of previous works can be fulfilled by consideration of the computational aspects follows by adding means of significant features and explicitly of scale. Thus, every scale-space blob includes explicit information about which gray-level blob with a relevant scale. The presented methodology in this research is general and can be applied for any features. Measuring significance behavior of features over a different range of the scale is one of the primary issues to address in case of speckle and noise presence. Via adding explicit gray level blob detection to raw Gaussian scale-space representation, the significance image can be obtained. The core of the proposed idea in this research is that L should reproduce the intrinsic characteristics of the gray level image, instead of some external criteria or optimized parameters. By this way, the data-driven model can: 1) detect significant features; 2) relation between these features at a different scale; 3) feature's occurrence scale.

The outline of this chapter organized as follows:
Section 3.2.2 provides the definition of a blob in the gray-level image follows by precise mathematic definition in section 3.2.3. The justification behind the idea of linking between gray-level blobs over scales into scale-space blobs to address previous problems is illustrated in section 3.2.4. Implementation of scale-space has done via sampled Gaussian kernel which results in a tree model; see section 3.2.5 and 3.2.6. In the section 3.2.7 of methodology chapter, a brief description of scale linking of a blob and common configurations to generate significance scale of each blob represented follows by scale refinement in section 3.2.7. Finally, significant blob with its effective scale has extracted based on scale-space blob volume and median set theory in sections 3.2.8, and 3.2.9 subsequently.

3.2.1. Scale-space representation (L)

The scale-space theory considers a stack of images as seen in Fig. 3.5 including the original image $\mathrm{f}(\mathrm{x},\mathrm{y})$ at the bottom of the Gaussian scale-space representation (Lindeberg, 1994). For an image $\mathrm{f}\colon \mathbb{R}^2 \to \mathbb{R}$, the scale-space representation $\mathrm{L}\colon \mathbb{R}^2 \times \mathbb{R}_+ \to \mathbb{R}$, at zero scale, is equal to the original image

$$L(x,y;0) = f,\ f(x,y)\ \forall\ (x,y) \in\ \mathbb{R}^2. \tag{3.6}$$

L is convolution $(*)$ of f with two-dimensional Gaussian kernel, and the result of the convolution operation is

$$L(x,y;t) = g(\xi,\eta;t) * \mathrm{f} = \iint_{(\xi,\eta)\in\mathbb{R}^2} \mathrm{f}(x-\xi, y-\eta)\ \ g(\xi,\eta;t)d\xi\ d\eta\ , t \geq 0. \tag{3.7}$$

As t is increasing, the spatial resolution of image decreases, and features suppress symmetrically. The input is two-dimensional image f resulting into a smoothed image from finer to coarser scale with different

scale level of features. The final image is smoothed one-parameter family of derived images (Fig. 3.5). The essential condition in the scale-space stack of images is that each feature at a coarse scale must have a response at a fine scale.

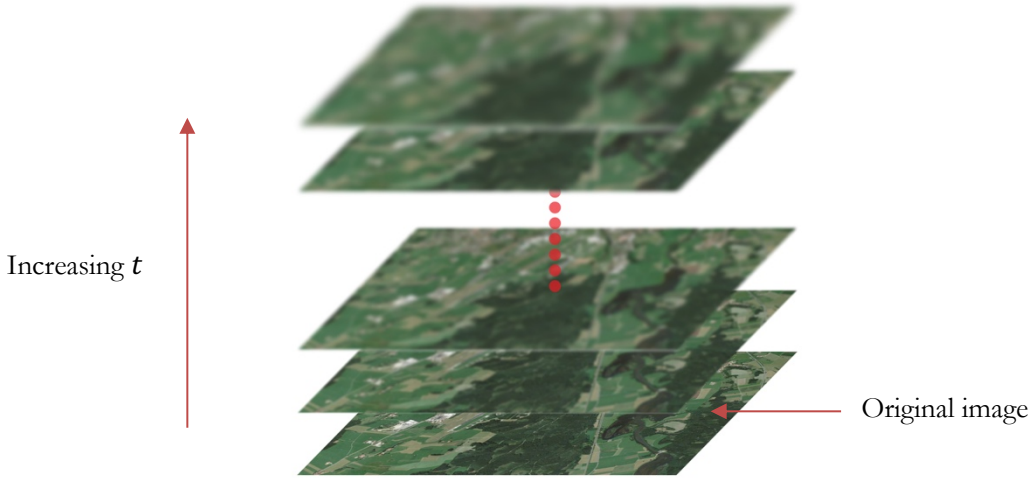

Fig. 3.5. Stack of images in scale-space representation. By increasing t the level of scale will be coarser.

The method uses the two-dimensional Gaussian smoothing function $g(x, y; t)$ (expression 2.1) to provide the multi-scale representation of the original image f from a fine scale to a coarse scale. Gaussian kernel ensures that features at coarser scale referred to features at finer scale, and no new artificial features will be created (Lindeberg, 1994). In addition, the convolution of one Gaussian kernel with a Gaussian kernel is another Gaussian kernel. Thus the L at coarse scale is computed from the convolution of g with L at a finer scale, successively. Scale parameter at the current scale or resolution image is shown by t and it corresponds to σ^2.

$$g(\xi, \eta; t) = \frac{1}{2\pi t}\, e^{-(\xi^2+\eta^2)/2t} \tag{3.8}$$

The local extrema regions in L across different scales is known as blob. There are several methods for blob detection that can be used with the Gaussian scale-space such as Laplacian of Gaussian, the difference of Gaussian, and determinant of Hessian. Furthermore, scale variation is playing a dominant role during scale-space blob detection. In the study investigated by Mahour et al. (2016) , scale-space blob detection done with the use of the determinant of Hessian

$$\det\ \mathcal{H}L(x, y; t) = t^2\left(L_{xx}L_{yy} - L_{xy}^2\right) \tag{3.9}$$

$\mathcal{H}L$ is the Hessian matrix of L. L_{xx}, L_{yy}, and L_{xy}^2 are second derivatives of L. The normalized scale of $\mathcal{H}L$ used for automatically scale selection. The local extrema of Hessian operator with respect to the object location in two-dimensional image function are assumed as blobs. Therefore, the $\mathcal{H}L$ detects a local maximum in scale-space among the three directions, i.e., space (x, y) and scale t, where it is

maximum in all three directions. t in the scale-space corresponds to the size of the tree radius (r), where $r = \sqrt{2t}$, and (x, y) determines the position of tree.

3.2.2. Definition of gray-level blob

The primary definition of blob can figure out directly from topological properties of a gray-level image. Blob is a connected region which is either considerably brighter or considerably darker than its background and neighborhood[17] (Lindeberg, 1994). The blob should have an adequately large area and remain stable over enough large interval in L. Thus, naturally, the blob with this definition should have some significance measure with it. In addition, the definition of scale-space blob with associated at least one local extremum that is arising in the L is related to gray-level blob as well. The basic idea of the blob is evident from Fig. 3.6. Simple definition is that let the blob grow spatially and include all lower gray-level values until it merges with another blob. Moreover, the image denotes that every blob in the two-dimensional surface is delimiting with one local extremum which gives rise to a blob, and a saddle point which extent a blob. It is essential to define gray-level blob extent and other characteristics. Therefore, from the precise mathematical definition of the gray-level blob and some blob descriptor quantities, ultimately generating significance image is possible.

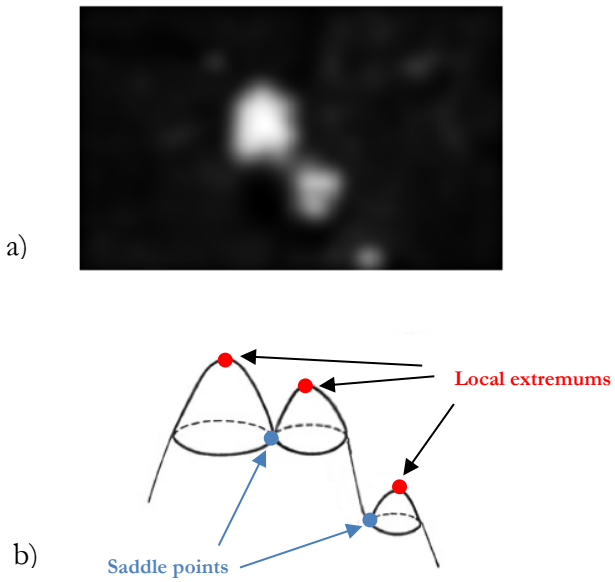

Fig. 3.6. Representation of gray-level blob definition a) The three bright gray-level blobs with the dark background at fixed level of scale. b) Schematic two-dimensional shape of the same three gray-level blobs at figure a (adapted from (Lindeberg & Eklundh, 1991)).

[17] There are separate systems correspond to the bright blob on dark background and dark blob on bright background.

3.2.3. Mathematical definitions of the blob descriptors

According to Lindeberg & Eklundh (1991) for the original gray-level image $f: \mathbb{R}^2 \rightarrow \mathbb{R}$ at a fixed level of scale, assume two local maximums $A, B \in \mathbb{R}^2$. $p_{A,B}$ is one of the infinite paths $(P_{A,B})$ between A, B, whereas the gray-level function along all these paths is assumed to be minimum. The base level Z_{base} of local extrema, A can be defined as

$$Z_{\text{base}}(A) = \{\max(B \in M)\ \max(p_{A,B} \in P_{A,B}) \min\{f(\xi, \eta), (\xi, \eta) \in p_{A,B}\}\} \tag{3.10}$$

where M is the set of all extremas. In addition, the support region of the blob A is the projection of all points $r \in \mathbb{R}^2$ which are more than the Z_{base}

$$G_{\text{support}}(A) = \{r \in \mathbb{R}^2 : \max(p_{A,B} \in P_{A,B}) \min\{f(\xi, \eta) \geq Z_{base}(A), (\xi, \eta) \in p_{A,B}\}\}. \tag{3.11}$$

The blob contrast definition gives by the difference between the local maximum and a base level of local maximum

$$c_{\text{blob}}(A) = f(A) - Z_{base}(A). \tag{3.12}$$

Eventually, the blob volume definition in three-dimension (i.e. spatial x, y and gray-level z) is

$$G_{\text{blob}}(A) = \{(x, y, z) \in \mathbb{R}^2 \times \mathbb{R} : \big((x, y) \in G_{support}(A)\big) \wedge \big(Z_{base}(A) < z \leq f(x, y)\big)\}. \tag{3.13}$$

The significance of the blob can be denoted based on the size of this volume which will be called the gray-level blob volume. The gray-level blob volume is an appropriate inherent property of the blob since it has both information on the spatial extent and signal amplitude.

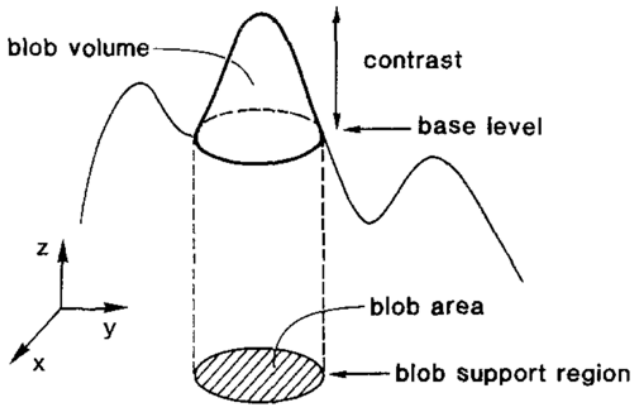

Fig. 3.7. Descriptive definitions of a gray-level blob in three directions of space (x, y), and gray-level(z): base level, area, support region, contrast, and volume (Source: Lindeberg & Eklundh, 1991).

3.2.4. The motivation for linking between gray-level blobs for tree CPA identification

In the scale-space representation for tree CPA detection, a set of smoothed images is just giving an implicit overview of tree profile gray-level values. On the other hand, giving a definition of gray-level blob at a fixed level of scale is not sufficient to extract image features. Explicit information in family of smoothed image related to gray level blobs and a relation between gray level blobs at different scale levels is required to prevent noise sensitivity. The gray-level blob at one fixed level is noise sensitive because of two or several local maximums which are located close to each other. Generally, these kinds of noise sensitivity lead to false detection. To be specific, this problem has been evident in the results of the previously applied scale-space methods concerning tree detection is related to trees with two or more sub crowns or close trees (Fig. 3.8). In this case, the scale-space feature detection at a fixed scale gives false several detections of the same tree. Linking between blobs of different scales is to determine significant blob based on image inherent properties. In other words, without prior knowledge about tree location, image scale, or shape of a tree[18]. By linking gray-level blobs over scale and consider their behavior we can obtain more stable descriptor, scale-space blobs.

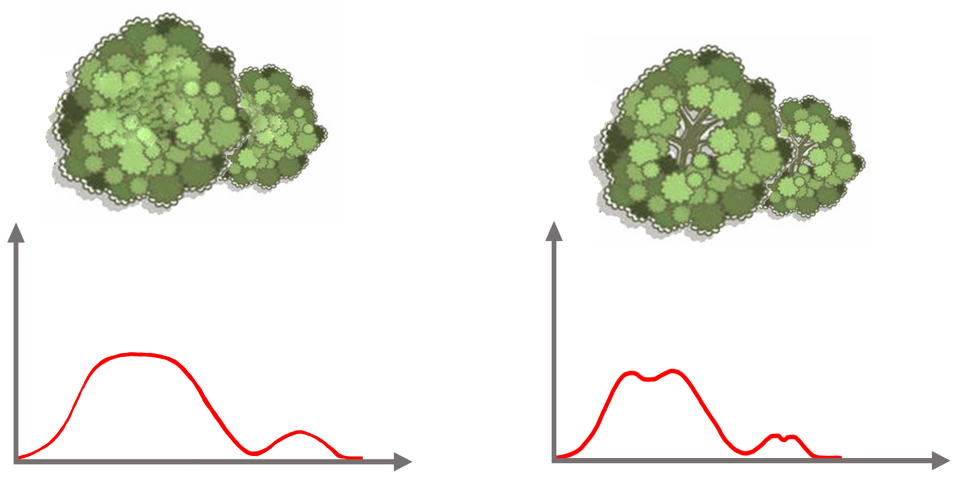

Fig. 3.8. Closely located trees, or trees with two sub-crowns. It leads to false detections at one fixed level of scale.

Therefore, defining a hierarchical relation between gray-level blobs over the scale, and use blob natural geometrical property to select significant blobs. Then by using scale-space, these properties can be converted to original descriptors. Thus, the closely located peaks at fine scale will be related to one peak with high gray-level blob volume at a coarser scale. The method calls 'scale-space blobs' with four-dimensional space (x, y), gray-level(Z), and scale (t).

3.2.5. Computational implementation of the scale-space

The definition of scale-space representation, which is presented in section 3.2.2, is continuous and therefore is impractical on discrete images since it is continuous. To apply scale-space on a discrete image, there are mainly two different approaches are generally used: the sampled Gaussian kernel, and the discrete Gaussian kernel. The difference between them becomes evident at a fine level of scale. Convolving the discrete image f with the sampled gaussian kernel is the simplest and straightforward approach to implement scale-space. The discrete Gaussian kernel is a more natural and refined approach

[18] Except assumption of bell-shaped for tree crowns.

to implement the scale-space theory on a discrete image. It gives a well-defined scale-space for discrete signals since the discrete scale-space only discretise the space coordinates. However, in blob detection from SAR images at fine level of scale there is a high effect of speckle. Thus, in the present study the implementation of scale-space has done via using the sampled Gaussian kernel.

3.2.6. Scale-space derivatives

Derivatives of scale-space representation can be applied at any level of scale in scale-space. Multi-scale spatial derivatives of L can be illustrated by

$$L_{x^n y^m}(x, y; t) = \partial_{x^n y^m} L(x, y; t) = g_{x^n y^m} * f \tag{3.14}$$

Where $g_{x^n y^m}$ indicates a $|n|, |m|$ orders of derivatives of the Gaussian kernel. Scale-space derivative can be computed by convolving Gaussian derivative operator with the original image f, bec ause of commutative property of the derivative operator with Gaussian kernel. The result of convolution in forms of explicit the integral is

$$\begin{aligned} L_{x^n y^m}(x, y; t) &= \int_{x'y' \in \mathbb{R}^N} g_{x^n y^m}(x - x', y - y'; t)\, f(x', y')\, dx'y' \\ &= \int_{x'y' \in \mathbb{R}^N} g_{x^n y^m}(x', y')\, f(x - x', y - y'; t)\, dx'y', \end{aligned} \tag{3.15}$$

and called 'the scale-space derivatives' of f at scale t.

3.2.7. Scale linking of blob and blob configurations

By linking the gray-level blobs at a fine level of scale with corresponding similar blob at a coarse level of scale, scale-space blobs will be derived (Lindeberg & Eklundh, 1991). Therefore, the object of interest will have four-dimensional volumes in scale-space, named as scale-space blob volume. Furthermore, each scale-space blob will have a minimum scale in which it is appearing and maximum scale in which it is disappearing. The difference between blob appearance scale and blob disappearance scale can be denoted as a scale-space blob lifetime; see Fig. 3.9. Blob lifetime denotes how long the blob can survive in scale-space.

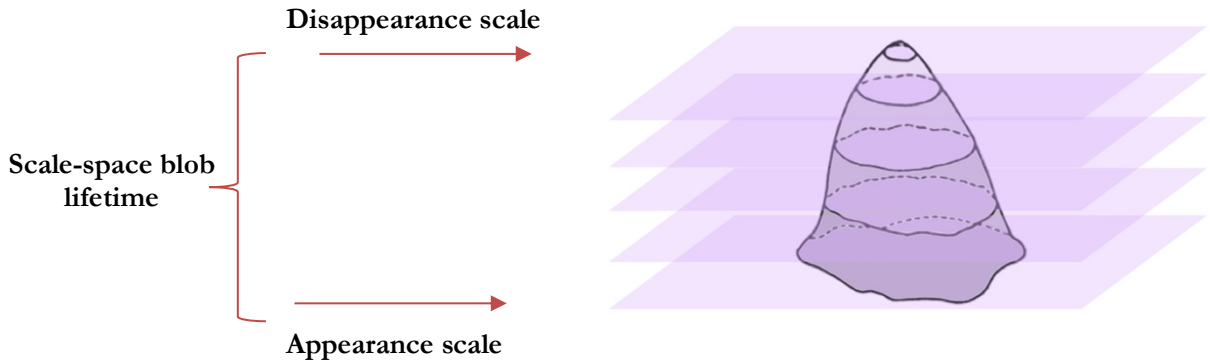

Fig. 3.9. Linking between gray-level blobs yields four-dimensional scale-space blobs with lifetime (adopted from Lindeberg & Eklundh, 1991).

During the linking bob at different scale levels, blob shape can change and may be distorted. In other words, different kinds of phenomenon can affect the topology of the blob. Blob can disappear, split, or merge over the blob scale linking. These kinds of events according to the catastrophe theory called bifurcations. Four possible bifurcation events can restrict the accomplishment of the blob-linking algorithm with increasing scale level (Fig. 3.10);

i. Annihilation: a blob disappears.
ii. Merge: two or more blobs merge into one blob.
iii. Split: one blob split into two blobs
iv. Create: a new blob appears[19]
v. Movement: blob can move

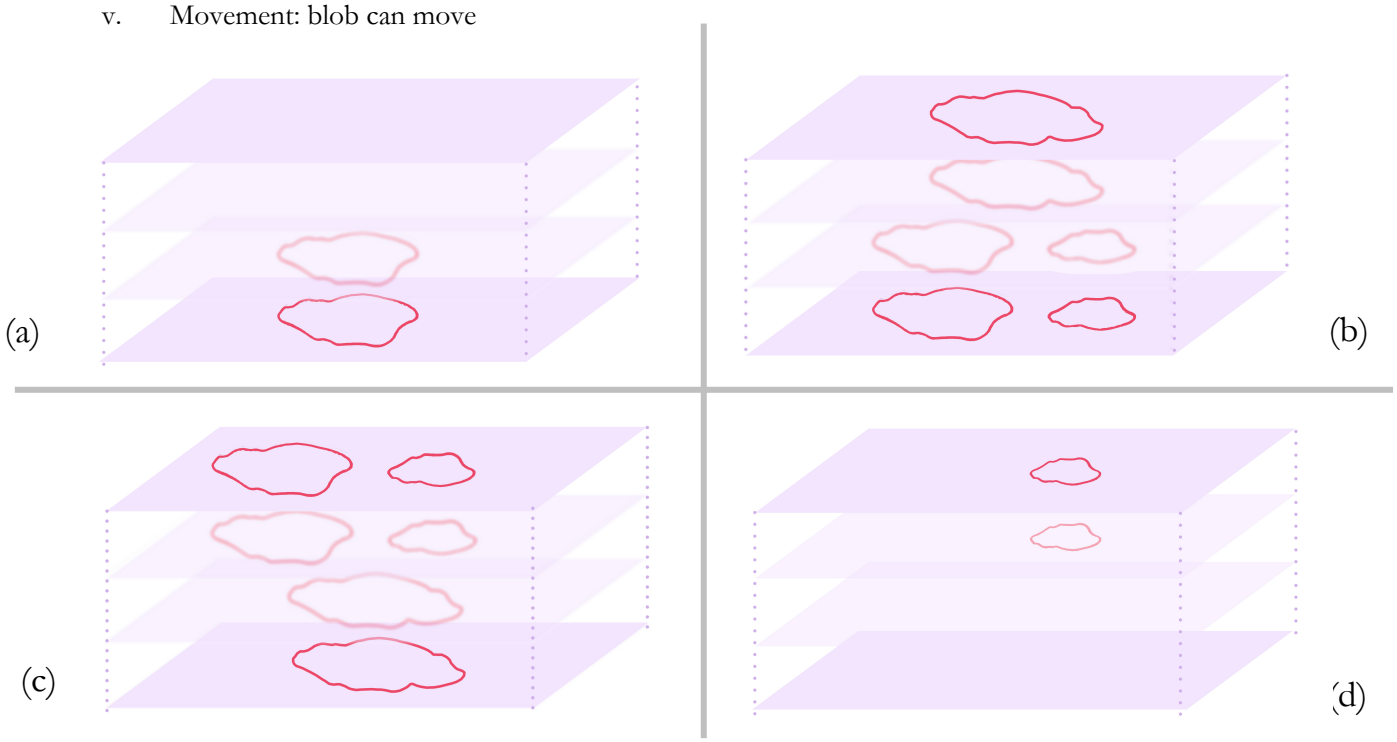

Fig. 3.10. Common four possible bifurcation events in scale-space: a) annihilation b) merge c) split d) create

3.2.8. Scale-space refinement

During the gray-level blob linking algorithm sometimes the interval between scales to relate a fine scale blob or blobs to coarse scale blob or blobs is too large. In this case, the smoothed scale is computed which means the number of scales will increase and all scales will shift by one.

3.2.9. Blob significance measurement and effective scale

To reach the final purpose of this study is intended structure extraction in the image, the methodology which can compare the significance of scale-space blobs in L over different levels of scale based on appearance and significance of blob is required. Referred to the blob descriptors definition which have

[19] The main cause is using numerical schemes to apply the scale-space theory on discrete image. since they don't have high volume or lifetime, they don't affect the final results.

gained until this section, in absence of any further prior knowledge, each four below-mentioned descriptors have the capacity to be considered as significance measure;

i. Blob support region: a blob with large spatial extent can be treated as more significant in comparison with a blob with a small spatial extent.

ii. Blob contrast: a blob having higher contrast can be treated as more significant in comparison with a blob with low contrast.

iii. Blob lifetime: a blob with a long lifetime in scale-space can be treated as more significant than a blob with a shorter lifetime.

iv. Blob volume: a blob with high blob scale-space volume can be treated as more significant than a blob with lower volume.

Among these nominated measurements, four-dimensional [20] scale-space volume in scale-space is considered as significance measure. The initial justification is that it consists of the spatial extent, the contrast and the blob lifetime. Moreover, scale-space blob volume calculated based on an effective scale notion. It means that for each high-volume scale-space indicate the scale where the gray-level blob volume is high. Then the gray-level blob support region of most significant blobs extracts which can determine tree CPA more precisely.

3.2.10. Effective scale based on random sets

After linking blobs preformation in L, we have multiple boundaries for the same gray-level blob at different scales. These multiple boundaries are modelled with random sets in this study. The coverage function according to Zhao (2012) of the spatial extent of all pixels in tree CPA boundary can be created as follows. The covering function and probability of pixels in $\mathbb{R}^2$ both are belonging to random set. If the pixel has be included in the boundary, then the covering function of it will be equal to 1 (e.g. centre point is always included). If half of the pixel is included in the boundary, then the covering function of the pixel will be 0.5. since we are dealing with set of pixels defined as tree CPA boundary, random set model can be created based on median of boundaries in $\mathbb{R}^2$. Therefore, median random set of multiple tree CPA boundaries with its representative scale, from random subsets in L can be computed. The median boundary of tree CPA also includes the representative scale.

3.3. Validation

The performance of individual tree CPA identification is divided into three types of uncertainty assessment. First, assessing the true detections. Second, validating the accuracy of the spatial extent of detected tree CPA. Third, assessing the geometrical position of the center of a detected tree. The relevant method to fulfill this section is illustrated precisely below.

[20] Space (x, y), gray-level (z), and scale (t).

3.3.1. Detection

Assessment of true individual tree detection has carried out based on the presence of tree or trees within the nominated subsets. Since the nominated subsets just contain limited recognizable trees, the visual assessment is sufficient. The red detected polygons which are false positive detections are known as error type 1. The trees which are not detected known as false negative detections, error type 2.

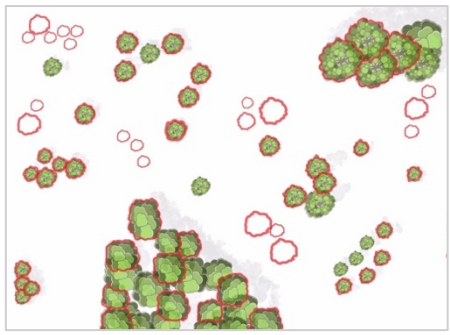

Fig. 3.11. Detection errors (false positive and false negative errors)

3.3.2. Spatial extension

To numerically assess the spatial boundary of detected individual trees, first manual visual digitization has done based on same F-SAR data. Since this research is fulfilled based on small subsets and the selected SAR image has a high spatial resolution, preferably same airborne F-SAR data has selected as reference data. In addition, considering tree crown as a varying object during the time, the same image would give a better result. Second, the percentage of overlap between the result segmentation and the polygon reference boundary has computed. If we consider A_0 as an area of reference tree CPA boundary, A_M area of median blob boundary, and A_{SS} as significance blob, then the area fit index AFI_M and AFI_{SS} according to Lucieer & Stein (2002) is

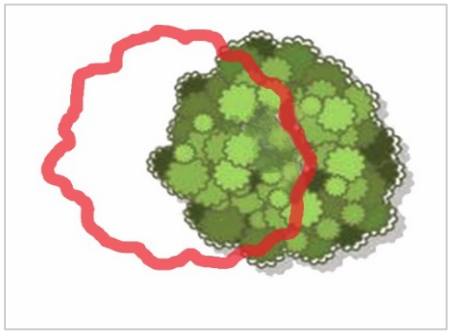

Fig. 3.12. Extensional error

$$AFI_M = \frac{A_0 - A_M}{A_0} \tag{3.16}$$

$$AFI_{SS} = \frac{A_0 - A_{SS}}{A_0} \tag{3.17}$$

Respectively. If the $AFI = 0.0$, then the overlap is best fit to reference tree CPA. If $AFI < 0.0$, then the reference tree CPA is undersegmented. Finally, if the $AFI > 0.0$ the reference tree CPA is oversegmented.

Furthermore, to evaluate the detection of tree CPA boundary, according to Yan et al. (2013) the overestimation and underestimation can be calculated as follow

$$\text{Overestimation} = 1 - \frac{\text{area}\,(A_i \cap A_0)}{\text{area}\,(A_i)} \tag{3.18}$$

$$\text{Underestimation} = 1 - \frac{\text{area}\,(A_i \cap A_0)}{\text{area}\,(A_0)} \tag{3.19}$$

The values of overestimation and underestimation which are close to 0, illustrate great agreement between reference tree CPA and significant blob. The total detection error which known as a root mean square (RMS) can be described as below

$$RMS = \sqrt{\frac{\text{overestimation}^2 + \text{underestimation}^2}{2}} \tag{3.20}$$

3.3.3. Position

The tree position defined by the geometry center position of tree CPA. Therefore, as reference data position of the center of present trees within the subsets carried out. Next the center position of converted vector polygons from three detections (i.e. scale-space blob, $\det \mathcal{H}L$, median set) have figure out. To assess the difference between each of these centroids (x, y) and reference tree crown centre (x_0, y_0), the Euclidean distance E is computed as below:

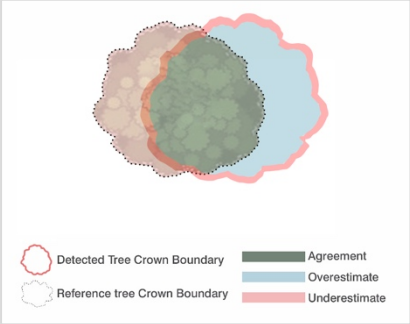

Figure 3.13. agreement assessment between reference and detected tree CPA

$$E_{SS} = \sqrt{(x_{SS} - x_o)^2 + (y_{SS} - y_o)^2} \tag{3.21}$$

$$E_M = \sqrt{(x_M - x_o)^2 + (y_M - y_o)^2} \tag{3.22}$$

$$E_H = \sqrt{(x_H - x_o)^2 + (y_H - y_o)^2} \tag{3.23}$$

Where the E_{SS}, E_M, and E_H are errors of detected scale-space, median set, and $\det \mathcal{H}L$ respectively.

4. STUDY AREA AND DATA DESCRIPTION

This section starts with introducing the study area of this research, and it is followed by providing a description of the available data.

4.1. Study area

One of the important factors in choosing the study area for each research is the availability of data. The study area is selected based on existing airborne SAR data which is provided by the Microwaves and Radar Institute of the German Aerospace Center (DLR). The reason for this selection was due to the value of this unique data (Horn et al., 2017) which is briefly illustrated below as well. Moreover, according to the focus of this study, the study area can be anywhere containing individual trees. The considered site is at the former military airfield of Kaufbeuren in the South of Germany, near Munich (Fig. 3.1). There are plenty of individual trees outside of the forest within the area of interest. Most of them located nearby the Barensee, roads, and buildings; see examples in Fig. 4.1.

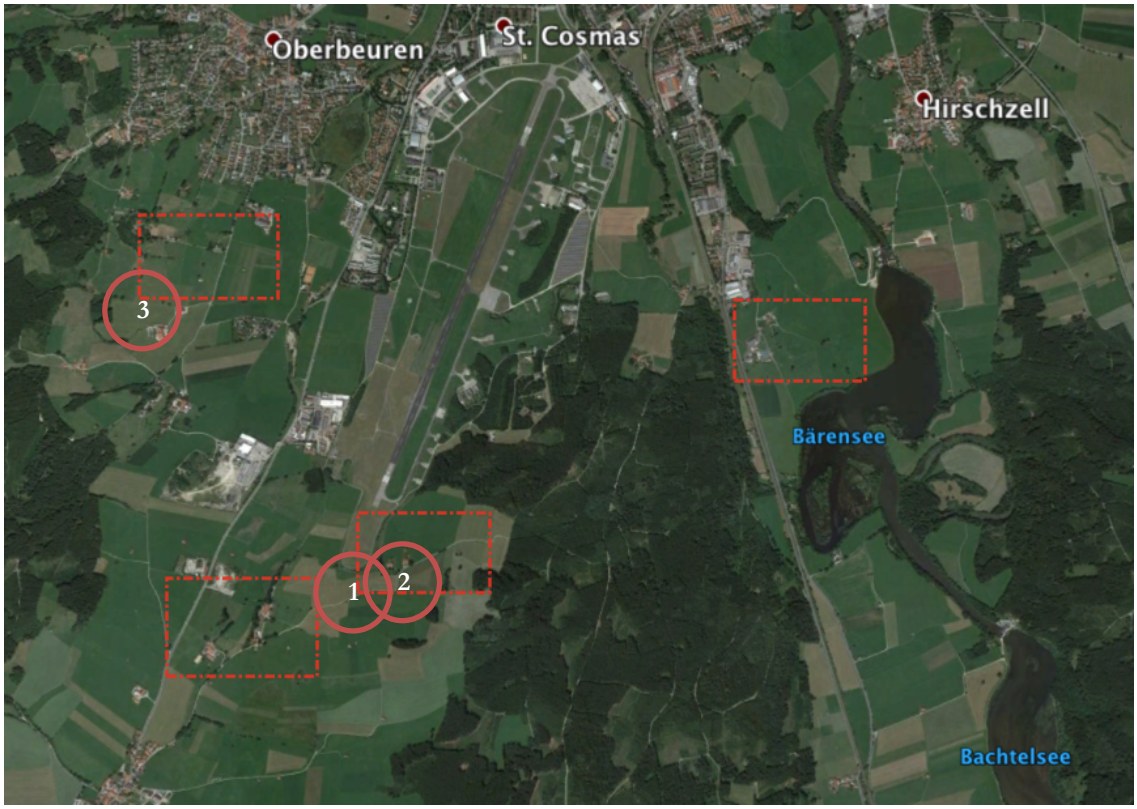

Fig. 4.1. The study area of interest near the Munich, Germany in 2014. The red rectangles provide the example spots with individual trees. The numbers are three nominated subsets which are presented in figure 3.2.

Source: Google Earth

For further analysis, three small subsets of the study area that contain two or three trees are extracted; see Fig. 4.2. The first subset is an individual tree next to the building house with grass background. This subset can provide information on how well the scale-space methods can distinguish between building and tree with low spectral separability with a background. The second subset is chosen due to the closeness of trees, so the capability of the scale-space in true detection of close trees can be assessed. Finally, the third subset is again an individual tree next to the building with another similar background (i.e. farm field).

Fig. 4.2. Three nominated subsets. They will name in text as subset 1, subset 2, and subset 3 respectively.

4.2. Remote sensing data image description

The available and considered data for this research based on the main objective consists of a fine spatial resolution SAR image. the F-SAR data includes two images of different months of the same year (Table. 4.1). The underlying assumption depends on the quality of available data is that tree crown boundaries do not change during two or three years. Whereas, the bound of extracted individual tree crown boundaries from different years can also be evaluated with the tree growth model. The brief description of technical characteristics and preparation of each dataset is mentioned below.

4.2.1. F-SAR data overview

The very high-resolution SAR images used for this research is multi-look airborne F-SAR. Recently, DLR has introduced the F-SAR, which is one of the latest and most of the most advanced airborne SAR instruments. This right-looking[21] SAR can acquire data in five fully polarimetric[22] frequency bands; X-, C-, S-, L- and P simultaneously. Furthermore, it provides a very high spatial resolution of up to 0.2 meters at X-band (Horn et al., 2017). Table 4.1 indicates that a summary of the technical characteristics of available F-SAR data.

[21] The interpretation of object's shadow also prove that the sensor is right-looking.
[22] F-SAR system has all 4 channels HH, HV, VH, VV.

Table 4.1 Characteristics of airborne F-SAR images

Date	20-Apr-2015			24-Jun-2015		
Bands	L	S	X	X	C	L
Frequency [MHz]	1325	3250	9600	9600	5300	1325
Polarizations	All bands are fully polarimetric					
Rg. resolution [m]	1.2	0.6	0.6	0.2	0.5	1.2
Az. resolution [m]	0.3	0.2	0.2	0.2	0.2	0.3

4.2.1.1. General properties

The F-SAR data provided by DLR for this research depends on the research goal, contains geocoded amplitude products and geocoded local incidence angle in radar geometry; see Tables ….. The amplitude, the intensity, and log-transformed image are easier to interpret, even despite speckle. Moreover, these images are preferred because of the lower dynamic range of the intensity which makes images more perceptible (Oliver & Quegan, 2004). The sounder mood of data is zero which indicates that the image is not acquired in nadir looking geometry. Moreover, the heading angle of the sensor is 91.164020, which denotes satellite look vector relative to the ground surface. Variety of product can be formed from the SAR data which known as 'complex image' based on the application at hand. For instance, the amplitude A, the phase ϕ, the intensity I[23], and the log intensity $\log I$.

The general information of whole data is that all images are geocoded to datum WGS-84 with UL Geo: 10 34' 51.27" E, 47 52' 31.06" N, and UL Map: 618211.000, 5303649.500. Moreover, the local incidence images based on terrain are available which gives incidence angle per pixel. The incidence angle varies from $57°$ to $71°$, with a mean of $64°$. From local incidence image and intensity image, calibrated intensity image can be obtained. The calibrated (log transformed) image is required to reduce restriction of low perception due to the large range of the intensity image.

[23] $I = A^2$, and the word "intensity" is synonymous with power or energy.

5. RESULTS

This chapter presents the results of a tree CPA delineation, as an object of interest, using the scale-space blob algorithm. These results are from three nominated subsets of the study area (section 4.1). Section 5.1 provides an overview of the scale-space blob algorithm. Section 5.2 presents the final results of the applied methods and significant blobs. Section 5.3 has allocated to the results of tree CPA delineation of subset 2 from different F-SAR wavelengths and their effect on outcomes. The final section presents the validation and comparison between the results of the scale-space blob methods and the scale-space method combined with $\det\mathcal{H}\mathrm{L}$blob detection algorithm. The minimum and maximum level of scale level in preformation of the scale-space algorithm selected initially based on a tree size in case of the image resolution.

5.1. Scale-space blob results

The scale-space blob detection algorithm to the Pauli decomposition results of the polarized FSAR data in L, S, X, and C bands image has applied. The first level of scale is containing a lot of small blobs due to the detection of the surface texture, additive noise of F-SAR images, and presence of the speckle (Fig. 5.1. a), whereas at coarse level of scale all image features become grouped into a single blob (Fig. 5.1. b)). The left images in Fig. 5.2, shows the gray level images. The top image is fine resolution image, whereas the below image is blurred image during scale-space analysis. The right images show the behavior of the gray-level blobs with increasing scale in the L. From these five images, it is apparent that by increasing scale, small blobs are disappearing gradually.

Blobs are disappearing much more quickly in the regions close to the steep intensity gradients[24]. These results highlighted that speckle can survive for a long time in L if they are located in regions with a lower gradient. Therefore, according to the definition of scale-space blob lifetime, blob lifetime cannot treat as an appropriate property for a significance measure. If the significance measure performs based on the scale-space blob lifetime, the results of blob significance are substantially overestimated. On the other hand, the findings provide an important evidence that the presence and effect of speckle in SAR images can be circumvented by the smoothing property of the scale-space, since speckle is always restricting the information extraction from image. Thus, during the scale-space there is no need to apply any speckle filter to reduce the speckle effect on image which make the analysis faster. The speckle reduction conducts automatically during the scale-space implementation. The effect of SAR additive noise is negatable, whereas it supressed by applying scale-space as well. Moreover, as we can see from Fig.5.2 the tree and house building are detected as single units at a coarse scale (blue arrows).

[24] Gray-level intensity is varying faster.

a)

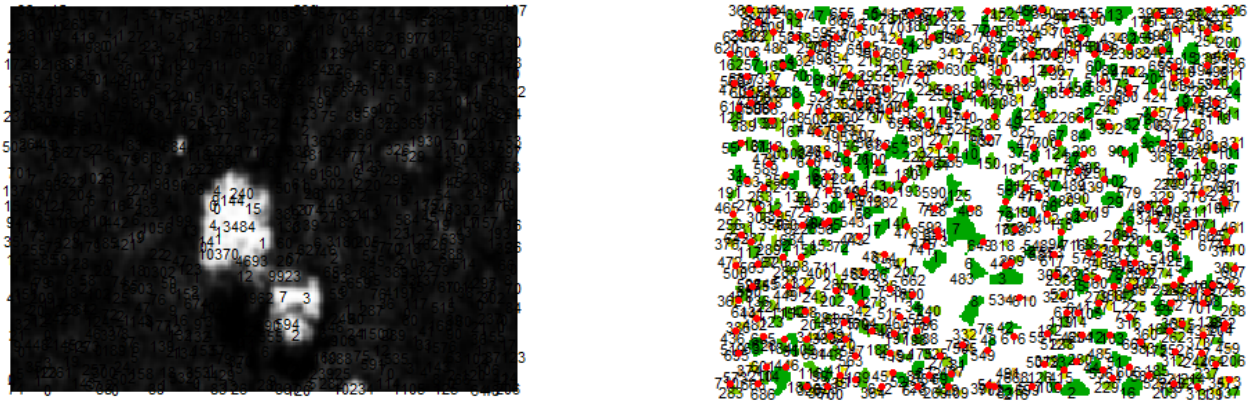

b)

Fig. 5.1. a) At the fine level of scale, a lot of small blobs appear due to the surface texture and presence of speckle b) At the coarse level of scale, the all features in the gray-level image appear as a single blob object.

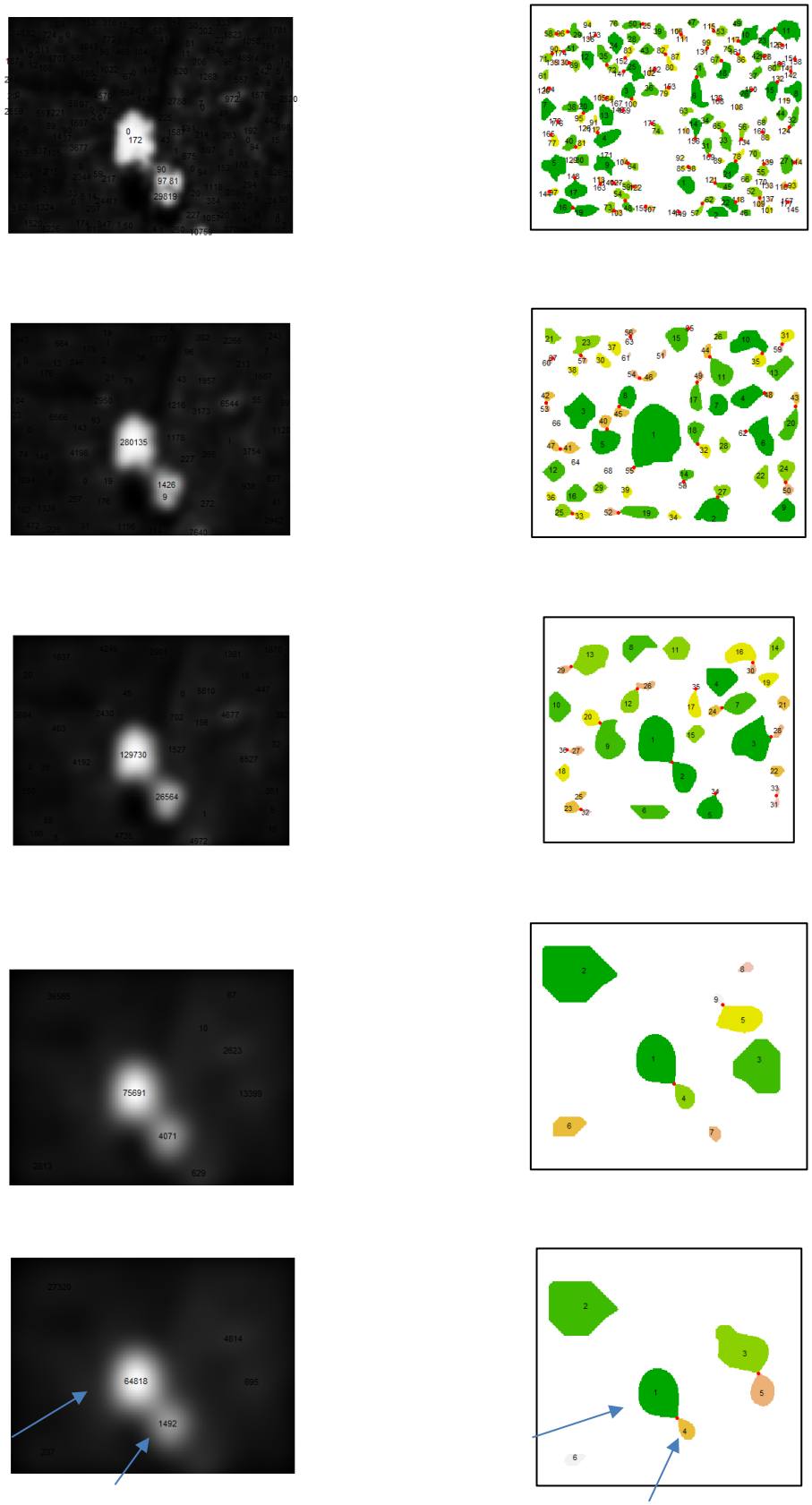

Fig. 5.2. Gray-level and gray-level blob images of the subset1, band L, F-SAR data at scale levels $t = 10$, $t = 28$, $t = 52$, $t = 145$, and $t = 178$ (from top to bottom). By increasing the scale level, the small blobs disappear gradually.

5.2. Raster to vector conversion

The images in Fig. 5.2. has shown blob at the fixed level of scale. The blob linking algorithms is cunducted to indicate significance blob in the L, without any prior knowledge about scale, position, or shape of tree crowns. The blob with high gray-level volume in scale-space after linking blob, resulted to the scale-space blob volume. Determination of a significant blob has done based on high scale-space blob volume. This blob denotes the accurate tree CPA boundary as well as its representative scale. To show the spatial relation between the blobs that related to the tree CPA at different levels of scale, blobs support regions at range of blob lifetime, are converted to vector boundaries. These boundaries have overlapped with the original F-SAR image to evaluate the best fit. Fig. 5.3. is presenting a significant blob related to the tree at their representative scale (i.e. yellow polygon). In addition, the median set blob has shown with green colour.

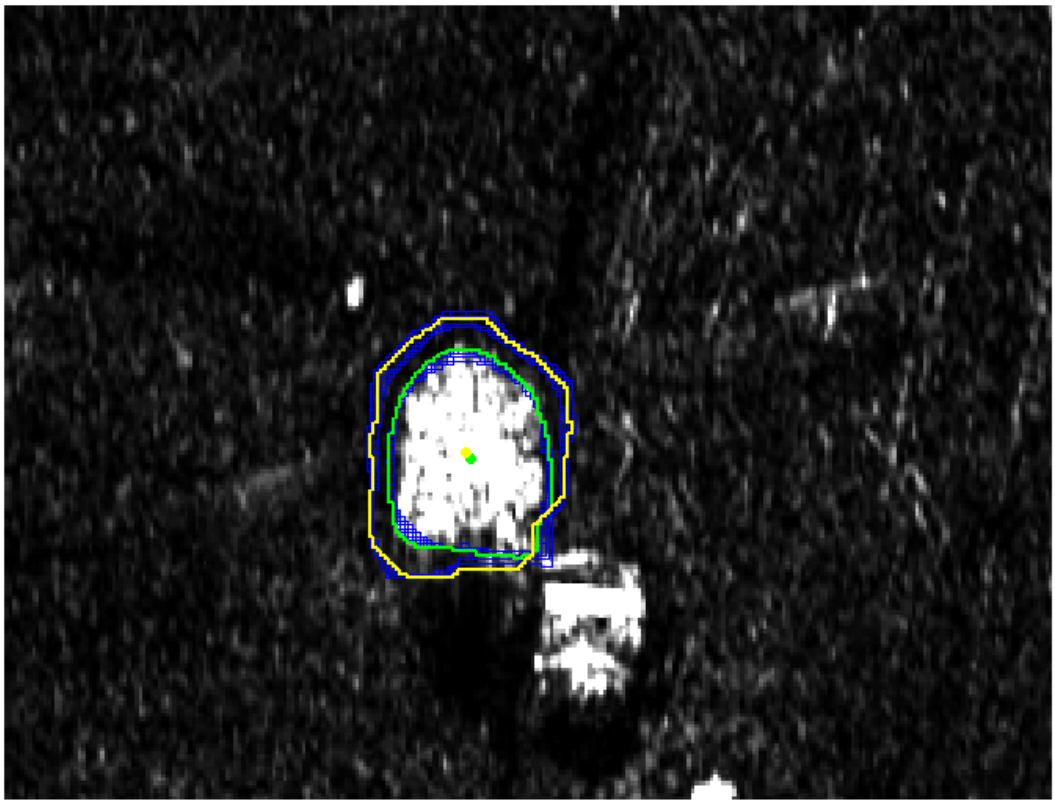

Figure 5.3. Vector boundaries (in blue) of high gray-level blob at different scales in scale-space representation. Green and yellow polygons are significant blob and median set, respectively.

5.3. Different wavelengths of F-SAR image

In Figs. 5.4, 5.5, 5.6, and 5.7 the results for four different bands of F-SAR data, subsets 3 has represented (bands L, S, C, and X respectively). Bands L (30-15 cm) and S (15-7.5 cm) with long wavelengths and high penetration ability provide better tree CPA identifications. However, C band (7.5-3.8 cm) and specifically X band (3.8-2.5 cm) with low penetration strength just provide above the surface of the tree crown.

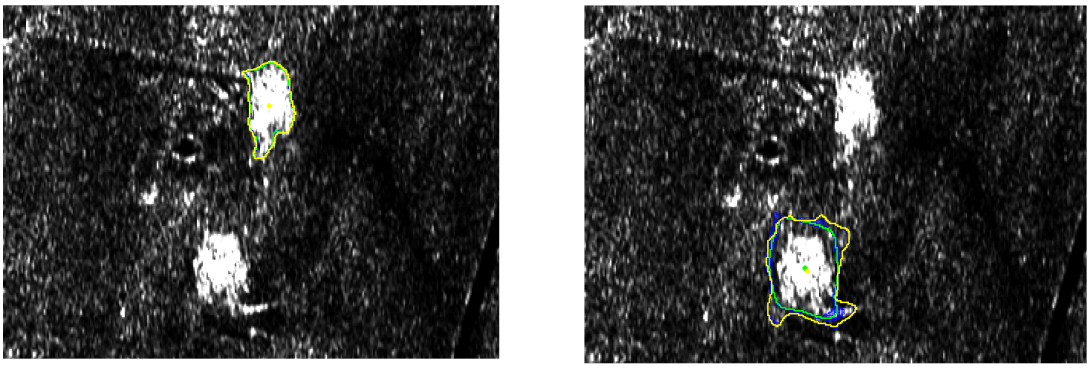

Figure 5.4. Subset 3, L-band, gray level blob support regions are shown by polygon.

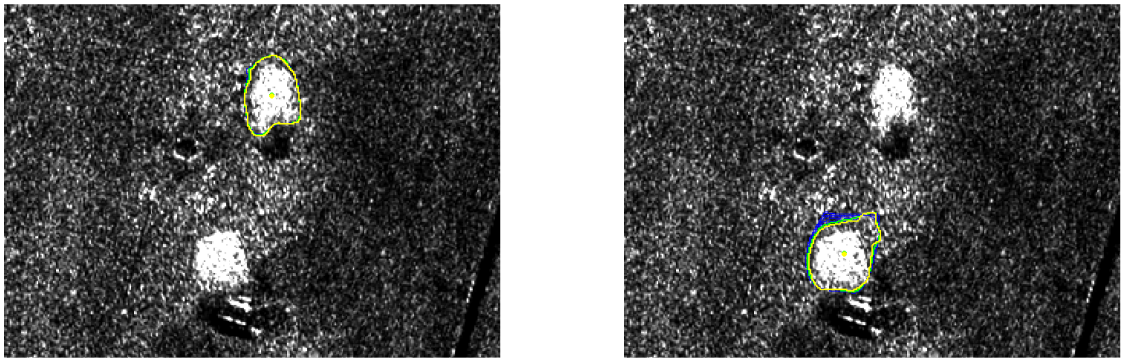

Figure 5.5. Subset3, S-band, gray level blob support regions are shown by polygon.

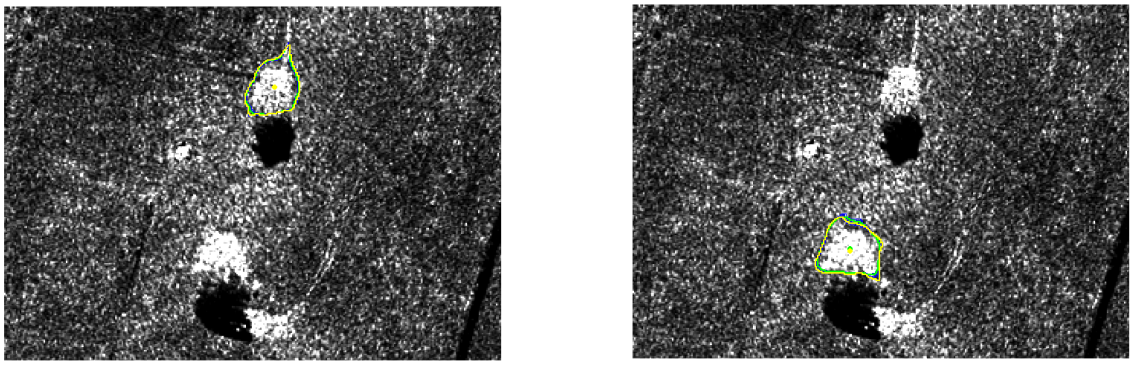

Figure 5.6. subset3, C-band, gray level blob support regions are shown by polygon.

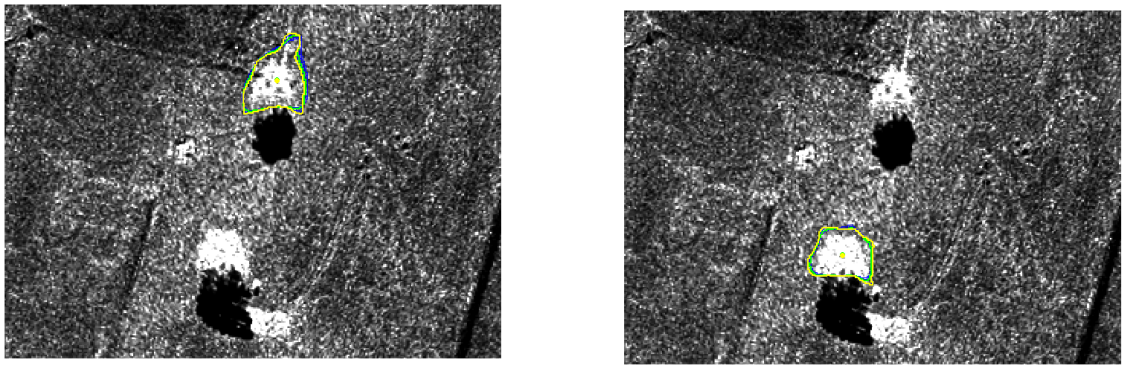

Figure 5.7. Subset3 X-band, gray level blob support regions are shown by polygon (all colors).

5.4. Validation

5.4.1. Detection accuracy

This section includes the comparison between the tree CPA detection result from the scale-space blob method and the $\det\mathcal{H}\mathrm{L}$. Both results are overlapped in the same image. As depicts from Fig. 5.8 $\det\mathcal{H}\mathrm{L}$ has several false positive errors and several overlapped close detections of the same tree at slightly different positions (seven detections). The method requires better thresholding which does not ensure 100% single true detection at the end. There are no criteria for this thresholding, and it is repeated until reach to the best result. In the other words, thresholding is a matter of try and error with possible better value always. However, the scale-space blob method detected the tree crown correctly.

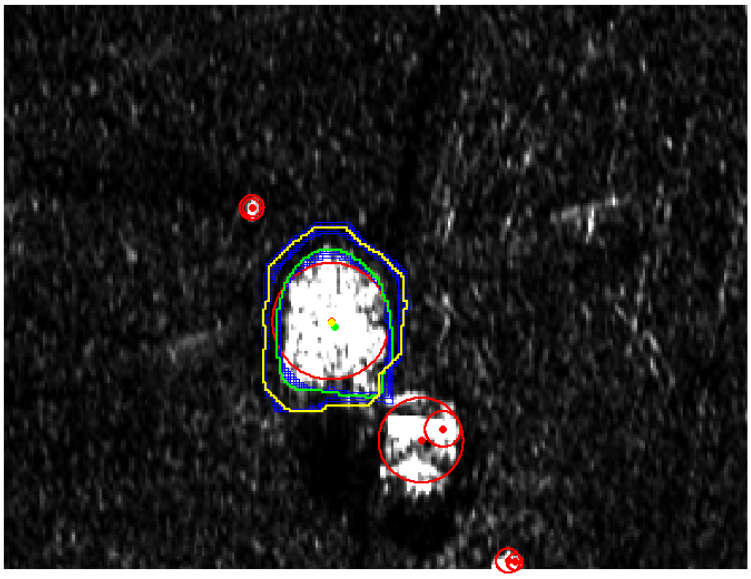

Fig. 5.8. Results of tree CPA detection from $\det\mathcal{H}\mathrm{L}$ (red circles), and the scale-space blobs (blue, yellow, and green lines), subset1.

As can see from Fig. 5.9, the preformation of the algorithm on overlapped adjacent trees results in false negative detections. Further experimental analysis is required to treat the meaning of significance blob based on critical points, effective scale, and rescaled blob volumes. Moreover, the range of scale level in analysis of the scale-space algorithm based on a tree size in case of the image resolution selected initially. However, in another feature detection, this minimum and maximum can be different.

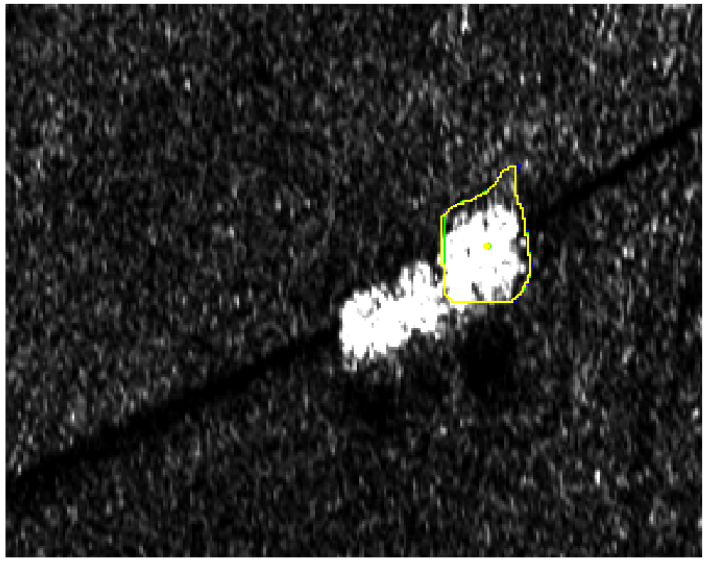

Fig. 5.9. Results of scale-space blob method on subset 3, which contains three close trees. It presents false negative detection of two trees.

5.4.2. Extensional accuracy

Since in this research, we obtained a more precise boundary of tree CPA as an irregular object, the comparison and validation of extensional accuracy have described between the results of the significant blob support region at representative scale and the support region of the median set blob at representative scale. Table 5.1 illustrates the difference between reference tree CPA area, and support regions of median set and significant blob. Both are under-segmented, whereas the spatial boundary of median set which also depicted from Fig 5.3 has lower area difference with reference boundary. Moreover, the lower overestimation and underestimation proves a good match between the support region of the median set blob and reference polygon boundary.

Table 5.1. Tree CPA extensional accuracy, L-band, subset1, difference between reference tree CPA boundary, median set, and significant blob support regions.

	$\mathbf{AFI_M(m^2)}$	$\mathbf{AFI_{SS}(m^2)}$	$\mathbf{AFI_{dH}(m^2)}$	**Overestimation**	**Underestimation**	**RMS**
Median set	-0.032			0.085	0.055	0.071
Significant blob		-0.556		0.360	0.004	0.254
Det Hessian			0.214	0.056	0.259	0.187

5.4.3. Positional accuracy

The positional accuracy has performed between centroids of reference tree CPA boundary, the significant blob, the median set blob, and $detHL$. The results of the errors are presented in Table 5.2. The assessments show the median set provides the more precise centre of the tree. The significant blob and $detHL$ have the same accuracy.

Table 5.2. Tree CPA positional accuracy between reference tree CPA center and the significant blob, median set, $detHL$.

	Centroids	Positional error (cm)
Reference	$(x_o, y_o) = (620503, 5301010)$	
The significant blob	$(x_{SS}, y_{SS}) = (620502.5, 5301012)$	$E_{SS} = 2.061$
The median set	$(x_M, y_M) = (620503.1, 5301011)$	$E_M = 1.004$
The $detHL$	$(x_H, y_H) = (620502.5, 5301012)$	$E_H = 2.061$

6. DISCUSSION

In this research, the automatic delineation of the tree CPA, based on the airborne F-SAR gray-level image by using well-founded multi-scale scale-space method delineated. The performance of this method in comparison to other data sources which can directly identify tree crown, such as Lidar and UAV, is much more efficient. The proposed method produced superior results without any assumption, classification, external criteria, or thresholding in relevant prior knowledge about tree neither shape of tree crown boundary, in contrast to, the previous investigated scale-space method. Including scale parameter in computations is crucial in terms of identifying features such as tree crown boundary which spatially varies according to image resolution. The support region of the high-volume scale-space provides information about

- The position and boundary extension of the tree on the ground
- The effective scale which can be treated in further analysis.

On the other hand, including the fourth dimension (i.e. gray-level value) increased the accuracy of tree detection concerning regions with poor spectral separability between tree crown and background surfaces.

From another point of view, this study demonstrates a feasible application of the scale-space blob method on SAR images, which so far has not explored. SAR system is an important data source with different capabilities regard to different data such as interferometry, different wavelengths, and different polarizations (Schmitt et al., 2013). Although the results give better segmentation of tree CPA in comparison to regular shapes, they are not adopted exactly to the tree crown boundaries. This quiet poor localization is due to the noise in relevant image spatial resolution. These kinds of slightly coarse but crucial information can be easily combined with either other vector, raster data in geographic information system (GIS), or other SAR data. Moreover, these data have the potential to combined with applied RS issues concerning different environmental issues. They can result in several applications such as tree biomass and volume estimation, canopy height model, tree monitoring, change detection, mapping tree health, irrigation management, and tree inventories.

In the present study, an assumption has been made to apply the proposed algorithm on three nominated subsets of the study area. The applicability of the proposed algorithm on the whole study area with many trees or on forest needs further investigations. As an example, though the scale-space blob algorithm offers more precise tree CPA boundary, in the identification of close trees faced some deficiencies.

The tree crown reference polygon has been digitized manually based on F-SAR data. First, the manual digitization of tree CPA would not be applicable for the large study areas with many trees. Second, UAV data or LiDAR data can be an alternative reference data source which is more precise, faster, and are applicable for a large area. However, in case of using different these kinds of data as reference data sources, two limitations must be considered. The first restriction is related to the high cost of UAV or Lidar data over large areas, whereas their accuracy is not too high in comparison manual delineation (Khosravipour, 2017). Second, in case of using different data from the input image, must be assumed tree crown boundary does not change over time.

To remove the effect of tree crown shadow, NDVI was used for optical images in previous studies (Ardila, 2012; Mahour, 2018). In the present study, shadow effect which is more evident in X-, and C-band images corrected via Pauli decomposition (Fig.5.6, 5.7). The Pauli decomposition has worked well enough, whereas using the RVI is not effective and does not provide the same results of removing shadow as NDVI on the optical image.

This research highlighted out that the capability of the scale-space method in individual tree detection as an object of interest. This complies with findings of previous related works (e.g. Brandtberg, 2002; Mahour et al., 2016; Mahour, 2018). We end up with higher detection accuracy (should be consider for small subset 1,3), higher extensional accuracy (considering extracting irregular tree CPA shape adopted with RMS 0.071cm for the median set and RMS 0.254cm for significance blob), and improved positional accuracy (1.004 Euclidian median set error and 2.061 for significant blob). These findings approve and comply with the scale-space blob method for feature detection without any prior knowledge or criteria and adding fourth-dimension gray-level value gives perceptually perfect results (Lindeberg & Eklundh, 1991).

In this study the scale-space blob methods cunducted on a high-resolution SAR data. The method is, however, applicable for tree crown identification from images of other sensors including different resolution active, passive, visible, near-infrared, panchromatic bands. Applying the method on coarse resolution dataset the extensional and position accuracy maybe decrease, whereas coarse structures (spectral profile) still can be detected. Different kinds of information based on data source and application can be obtained. Various image features depend on an application at hands such as ridges, edges, corners, and blobs can be detected using the scale-space blob algorithm. As an example, the scale-space method can be used to detect important features from ultrasound images to asses tumor growth.

Different types of development in science can restrict the application of the proposed scale-space method. One of the significant developments is related to a data source. In modern surveying, by improvement of laser scanners maybe there will be an opportunity to individual trees 3D mapping directly.

7. CONCLUSION AND FURTHER ANALYSIS

7.1. Conclusion

This research has proposed and implemented a multiscale representation of gray-level high-resolution F-SAR image to automatic scale selection and trees CPA extraction. The scale-space blob method is the well-founded bottom-up method, without requirements of any prior knowledge, assumption, criteria, or tuning parameter about tree crown shape. It uses just a qualitative description of the gray-level image to determine the approximate position of the tree, the spatial extent of tree CPA, and representative scale. The tree CPA boundary identification is based on the well-defined notion of a blob. The blob linking algorithm can generate the multi-scale representation of blobs with reference to the tree crown at the original image. The significant blob with high gray-level volume in scale-space representation blob can provide natural geometrical information of tree crown. Results signified that good agreement between reference data and significance blob. These data can be combined with GIS data or different SAR data to address different environmental issues.

The scale-space theory treats the tree crown as a multi-scale object on discrete SAR image perfectly. The smoothing property of the method treats perfectly with the presence of speckle with gamma distribution in the SAR image (refer to Fig. 5.2). Different bands of F-SAR image based on their frequency and penetration strength provides slightly different accuracy information. Depends on an application at hand, each wavelength can be preferred.

The detection accuracy for small subsets 1, 3 with single trees, results true detections. Extensional accuracy, considering extracting irregular tree CPA, obtained with RMS 0.071 for the median set and RMS 0.254 for significance blob. The positional accuracy (1.004 Euclidian median set error and 2.061 for significant blob) is also improved in case of choosing the best boundary at its effective scale. The representation of blob related to tree crown in different scale levels stresses that all levels of scale should be taken into account in the implementation of scale-space. The straightforward and robustness of this method presents the potential of it to apply on different VHR passive or active data sources from different platforms. Further investigations are required to choose significant blob more precisely to get the best boundary of tree CPA, and better detection of adjacent tree crowns.

With this work we aimed to explore the possibility of applying the scale-space methods on SAR data, considering the presence of speckle. In addition, making scale parameter explicit in scale-space representation via using a gray-level image. the presented algorithm can assist other scientists, or stakeholders for different feature detection from different data sources.

7.2. Recommendations for further analysis

The number of selected high-volume scale-space blobs are arbitrary, whereas there is a well-defined ranking algorithm between the blobs. The most significant blobs stand out in comparison to other blobs. It would be great if there is an appropriate justification in general situations. Furthermore, to treat the significant blob better, the notion of effective scale and transformed blob volume could be considered in the calculation of the scale-space blob for each scale-space blob.

LIST OF REFERENCES

Anfinsen, S. N., Doulgeris, A. P., & Eltoft, T. (2009). Estimation of the Equivalent Number of Looks in Polarimetric Synthetic Aperture Radar Imagery. *IEEE Transactions on Geoscience and Remote Sensing*, *47*(11), 3795–3809. https://doi.org/10.1109/TGRS.2009.2019269

Ardila, J. P. (2012). *Object-based methods for mapping and monitoring of urban trees with multitemporal image analysis*. Published doctoral dissersion University of Twente Faculty of Geo-Information and Earth Observation (ITC).

Ardila, J. P., Bijker, W., Tolpekin, V. A., & Stein, A. (2012a). Context-sensitive extraction of tree crown objects in urban areas using VHR satellite images. International Journal of Applied Earth Observation and Geoinformation, 15, 57–69. doi:10.1016/j.jag.2011.06.005

Ardila, J. P., Bijker, W., Tolpekin, V. A., & Stein, A. (2012b). Multitemporal change detection of urban trees using localized region-based active contours in VHR images. Remote Sensing of Environment, 124, 413– 426. doi:10.1016/j.rse.2012.05.027

Balzter, H. (2001). Forest mapping and monitoring with interferometric synthetic aperture radar (InSAR). *Progress in Physical Geography*, *252*, 159–177. doi:10.1177/030913330102500201

Bellefontaine, R., Food and Agriculture Organization of the United Nations., & CIRAD (Organization). (2002). *Trees outside forests : towards better awareness*. International Cooperation Centre on Agrarian Research for Development and Food and Agriculture Organization of the United Nations. Retrieved from http://www.fao.org/docrep/005/Y2328E/Y2328E00.HTM

Brandtberg, T. (2002). Individual tree-based species classiÿcation in high spatial resolution aerial images of forests using fuzzy sets. *Fuzzy Sets and Systems*, *132*, 371–387.

Brandtberg, T., & Walter, F. (1998). Automated delineation of individual tree crowns in high spatial resolution aerial images by multiple-scale analysis. *Machine Vision and Applications*, *11*(2), 64–73. https://doi.org/10.1007/s001380050091

Dida, J. J. V., Paquit, J. C., Boongaling, C. G. K., Magnaye, G. E., & Bantayan, N. C. (2013). Assessment of Trees Outside Forest (TOF) in Selected Makiling Subwatersheds. *International Journal of Agriculture System*, *1*(2), 104–111.

Sakshaug, S. (2013). *Evaluation of Polarimetric SAR Decomposition methods for tropical forest analysis EOM-3901*- Master Thesis in Energy, Climate and Environment.

Gomes, M. F., & Maillard, P. (2016). *Detection of Tree Crowns in Very High Spatial Resolution Images*. In Environmental Applications of Remote Sensing. doi: 10.5772/62122

Gschwantner, T., Schadauer, K., Vidal, C., Lanz, A., Tomppo, E., di Cosmo, L., … Lawrence, M. (2009). Common tree definitions for national forest inventories in Europe. *Silva Fennica*, *43*(2). https://doi.org/10.14214/sf.463

Horn, R., Jaeger, M., Keller, M., Limbach, M., Nottensteiner, A., Pardini, M., … Scheiber, R. (2017). F-SAR - Recent upgrades and campaign activities. *Proceedings International Radar Symposium*, 2–11. https://doi.org/10.23919/IRS.2017.8008092

Izzawati, Wallington, E. D., & Woodhouse, I. H. (2006). Forest height retrieval from commercial X-band SAR products. *IEEE Transactions on Geoscience and Remote Sensing*, *44*(4), 863–870. https://doi.org/10.1109/TGRS.2006.870828

Keller, M., Fischer, J., Datum, M. J., Ponce, O., Reigber, A., & Aerospace, G. (2016). *DLR's Airborne SAR System F-SAR PRODUCT DESCRIPTION*.

Khosravipour, A. (2017). Detection individual trees from Lidar. Published doctoral dissersion University of Twente Faculty of Geo-Information and Earth Observation (ITC). https://doi.org/10.3990/1.9789036543965

Koch, B. (2010). Status and future of laser scanning, synthetic aperture radar and hyperspectral remote sensing data for forest biomass assessment. *ISPRS Journal of Photogrammetry and Remote Sensing*, *65*, 581–590. https://doi.org/10.1016/j.isprsjprs.2010.09.001

Larsen, M., Eriksson, M., Descombes, X., Perrin, G., Brandtberg, T., & Gougeon, F. A. (2011). Comparison of six individual tree crown detection algorithms evaluated under varying forest conditions. *International Journal of Remote Sensing*, *32*(20), 5827–5852. https://doi.org/10.1080/01431161.2010.507790

Lee, J.-S., & Pottier, E. (2009). *Polarimetric Radar Imaging* (Vol. 143). CRC Press. https://doi.org/10.1201/9781420054989

Lee, J., Grunes, M. R., Pottier, E., & Ferro-famil, L. (2004). Polarimetric Scattering Characteristics. *Terrain*, *42*(4), 722–731.

Lin, W., Meng, Y., Qiu, Z., Zhang, S., & Wu, J. (2017). Measurement and calculation of crown projection area and crown volume of individual trees based on 3D laser-scanned point-cloud data Measurement and calculation of crown projection area and crown volume of individua. International journal of remote sensing. doi: 10.1080/01431161.2016.1265690

Lindeberg, T. (1994). *Scale-Space Theory in Computer Vision*. Boston, MA: Springer US. https://doi.org/10.1007/978-1-4757-6465-9

Lindeberg, T., & Eklundh, J.-O. (1991). On the computation of a scale-space primal sketch. *Journal of Visual Communication and Image Representation*, *2*(1), 55–78. https://doi.org/10.1016/1047-3203(91)90035-E

Loong, C. K., Kanniah, K. D., & Pohl, C. (2013). Oil Palm Tree Height Estimation Using InSAR, 2–5. Retrieved from http://www.a-a-r-s.org/acrs/administrator/components/com_jresearch/files/publications/Ab 0061.pdf

Lucieer, A., & Stein, A. (2002). Existential uncertainty of spatial objects segmented from satellite sensor imagery. *IEEE Transactions on Geoscience and Remote Sensing*, *40*(11), 2518–2521. https://doi.org/10.1109/TGRS.2002.805072

Mahour, M. (2018). Scaling of remote sensing information for orchard management. https://doi.org/10.3990/1.9789036546898

Mahour, M., Tolpekin, V., & Stein, A. (2016). Tree detection in orchards from VHR satellite images using scale-space theory. In L. Bruzzone & F. Bovolo (Eds.). International Society for Optics and Photonics. https://doi.org/10.1117/12.2241529

Marr, D. (1982). Understanding Complex Information-processing Systems. *W. H. Freeman and Com- Pany,* (1956).

Mercer, B., Zhang, Q., Schwaebisch, M., & Denbina, M. (2010). Estimation of forest biomass from an airborne single-pass L-band pol-InSAR system. *International Archives of the Photogrammetry, Remote Sensing and Spatial Information Sciences*.

Neumann, M., Ferro-Famil, L., & Reigber, A. (2010). Estimation of Forest Structure, Ground, and Canopy Layer Characteristics From Multibaseline Polarimetric Interferometric SAR Data. *IEEE Transactions on Geoscience and Remote Sensing*, *48*(3), 1086–1104. https://doi.org/10.1109/TGRS.2009.2031101

Nicolaescu, L., & Oroian, T. (2001). Radar cross section. In *5th International Conference on Telecommunications in Modern Satellite, Cable and Broadcasting Service, TELSIKS 2001 - Proceedings of Papers* (Vol. 1, pp. 65–68). IEEE. https://doi.org/10.1109/TELSKS.2001.954850

Olesk, A., Praks, J., Antropov, O., Zalite, K., Arumäe, T., & Voormansik, K. (2016). Interferometric SAR Coherence Models for Characterization of Hemiboreal Forests Using TanDEM-X Data. *Remote Sensing*, *8*(9), 700. https://doi.org/10.3390/rs8090700

Oliver, C., & Quegan, S. (2004). *Understanding synthetic aperture radar images*. SciTech Publ.

OpenForests. (n.d.). Retrieved December 27, 2018, from https://openforests.com

Polarimetric Decompositions. Coherent Decompositions 4.1.1 Purpose of the Coherent Decompositions. (n.d.).

Pu, R., & Landry, S. (2012). A comparative analysis of high spatial resolution IKONOS and WorldView-2 imagery for mapping urban tree species. *Remote Sensing of Environment*, *124*(September), 516–533. https://doi.org/10.1016/j.rse.2012.06.011

Ramezani, M. (2015). Urban tree species classification based on spectral profile of crowns and texture.

Schmitt, M., Brück, A., Schönberger, J., & Stilla, U. (2013). Potential of Airborne Single-Pass Millimeterwave InSAR Data for Individual Tree Recognition. In *DGPF Tagungsband* (Vol. 22, pp. 427–437). Retrieved from http://www.pf.bv.tum.de

Schmitt, M., Shahzad, M., & Zhu, X. X. (2015a). Reconstruction of individual trees from multi-aspect TomoSAR data. *Remote Sensing of Environment*, *165*(August), 175–185. https://doi.org/10.1016/j.rse.2015.05.012

Schmitt, M., Shahzad, M., & Zhu, X. X. (2015b). Reconstruction of individual trees from multi-aspect TomoSAR data. *Remote Sensing of Environment*, *165*, 175–185. https://doi.org/10.1016/J.RSE.2015.05.012

Shah, S. K., Hussin, Y. A., & van Leeuwen, L. M. (2011). Modelling the relationship between tree canopy projection area and above ground carbon stock using high resolution geoeye satellite images. In *ACRS 2011 : proceedings of the 32nd Asian conference on remote sensing : sensing for Green Asia, 3-7 October 2011, Taipei, Taiwan* (p. 6).

Tolpekin, V. A., Ardila, J. P., & Bijker, W. (2010). Super-Resolution Mapping for Extraction of Urban Tree Crown Objects From Vhr Satellite Images. *The International Archives of the Photogrammetry, Remote Sensing and Spatial Information Sciences.*

USDA. (2002). Watching and acting together: Concurrent plan recognition and adaptation for human-robot teams. https://doi.org/10.1126/science.3.72.734-a

Varekamp, C. (2001). *Canopy reconstruction from interferometric {SAR}*.

Vashum, K., & Jayakumar, S. (2012). Methods to Estimate Above-Ground Biomass and Carbon Stock in Natural Forests - A Review. *Journal of Ecosystem & Ecography*, *02*(04), 1–7. https://doi.org/10.4172/2157-7625.1000116

Wulder, M., Niemann, K. O., & Goodenough, D. G. (2000). Local maximum filtering for the extraction of tree locations and basal area from high spatial resolution imagery. *Remote Sensing of Environment*, *73*(1), 103–114. https://doi.org/10.1016/S0034-4257(00)00101-2

Yadav, Y., Bahadur, B., Chhetri, K., Raymajhi, S., Rajtiwari, K., & Kumar Sitaula, B. (2017). *International Peer-Reviewed Journal ISSN 2321 3655 Oct. Jour. Env.*

Yan, L., Scarborough, J., Gong, P., Holt, A., & Clinton, N. (2013). Accuracy Assessment Measures for Object-based Image Segmentation Goodness. *Photogrammetric Engineering & Remote Sensing*, *76*(3), 289–299. https://doi.org/10.14358/pers.76.3.289

Zhang Li-fu, Lu Dong-fang, YUAN Ming, CAO Li-wen, L. G. (2011). Research on 3D Laser Scanning Technology and Its Application in Forestry Survey--《Forestry Machinery & *Forestry Machinery & Woodworking Equipment*.

Zhao, X. (2012). *Random sets to model uncertainty in remotely sensed objects*. Published doctoral dissersion University of Twente Faculty of Geo-Information and Earth Observation (ITC).